Guiding center motion in tokamaks

BY YOUJUN HU

Institute of plasma physics, Chinese Academy of Sciences
Email: yjhu@ipp.cas.cn

Abstract

This note discusses numerical computation of guiding center orbits in tokamaks using the cylindrical coordinates and several magnetic coordinates. Some subtle things involved in using a particlular kind of magnetic coordinates called field-line-following coordinates are discussed (I am using this kind of coordinates in developing a new module in GEM code). We assume a general tokamak magnetic field speccified numerically (provided by the EFIT G-file). This note is evolving, begining with my first try of computing guiding-center motion in Solovev analytical equilibrium using cylindrical coordinates, and then extending to general numerical magnetic field, and later using magnetic coordinates.

1 Equations of guiding-center motion

The equations of guiding center motion are written[1] (refer to my notes "collisionless_drift_kinetic_equation.tm" for the derivation)

$$\frac{d\mathbf{X}}{dt}\equiv \mathbf{v}_d=\frac{\mathbf{B}^\star}{B_\parallel^\star}v_\parallel+\frac{\mu}{m\Omega B_\parallel^\star}\mathbf{B}\times\nabla B+\frac{1}{BB_\parallel^\star}\mathbf{E}\times\mathbf{B} \tag{1}$$

$$\frac{dv_\parallel}{dt}=-\frac{\mu}{m}\frac{\mathbf{B}^\star}{B_\parallel^\star}\cdot\nabla B+\frac{Ze}{m}\frac{\mathbf{B}^\star}{B_\parallel^\star}\cdot\mathbf{E} \tag{2}$$

where $\mathbf{X}$ is the guiding-center position, $v_\parallel$ is the parallel (to the magnetic field) velocity, m and Ze are the mass and charge of the particle, respectively, μ is the magentic moment defined by $\mu=mv_\perp^2/(2B)$ with $v_\perp$ being the pependicular speed; $\Omega=BZe/m$ is the cyclotron angular frequency, $\mathbf{B}^\star$ and $B_\parallel^\star$ are defined by

$$\mathbf{B}^\star=\mathbf{B}+B\frac{v_\parallel}{\Omega}\nabla\times\mathbf{b}, \tag{3}$$

$$B_\parallel^\star\equiv\mathbf{b}\cdot\mathbf{B}^\star=B\Big(1+\frac{v_\parallel}{\Omega}\mathbf{b}\cdot\nabla\times\mathbf{b}\Big), \tag{4}$$

respectively, where $\mathbf{b}=\mathbf{B}/B$. If using approximation $B_\parallel^\star\approx B$, then

$$\frac{d\mathbf{X}}{dt}=v_\parallel\mathbf{e}_\parallel+\mathbf{V}_D=v_\parallel\mathbf{b}+\underbrace{\frac{v_\parallel^2}{\Omega}\nabla\times\mathbf{b}}_{\text{curvature drift}}+\underbrace{\frac{\mu}{m\Omega B}\mathbf{B}\times\nabla B_0}_{\nabla B\text{ drift}}+\underbrace{\frac{1}{B^2}\mathbf{E}\times\mathbf{B}}_{E\times B\text{ drift}}. \tag{5}$$

[Before getting to know the above form of the equations of the guiding-center motion, I used the following form of the equations (refer to my notes "collisionless_drift_kinetic_equation.tm"):

$$\frac{d\mathbf{X}}{dt}=\mathbf{b}v_\parallel+\frac{1}{\Omega}\mathbf{b}\times\Big(\frac{\mu}{m}\nabla B+v_\parallel^2\boldsymbol{\kappa}-\frac{Ze}{m}\mathbf{E}\Big), \tag{6}$$

$$\frac{dv_\parallel}{dt}=-\frac{\mu}{m}\mathbf{b}\cdot\nabla B+\frac{v_\parallel\mu}{m\Omega}\boldsymbol{\kappa}\cdot\mathbf{b}\times\nabla B+\frac{Ze}{m}\mathbf{b}\cdot\mathbf{E}, \tag{7}$$

which does not converve the toroidal angular momentum P_ϕ excatly in an axisymmetrical equilibrium magnetic field (this has been tested numerically) while the new form given in Eqs. (1)-(4) can conserve P_ϕ excatly. Besides to be more accurate, the new form is compact and convenient for numerical implementation.] My latest numerical code uses Eqs. (1)-(4) as the the equations of guiding center motion.

1.1 Define new units

The above formulas are in SI units, which are good since SI units are getting widely used, and thus these formulas are accessible to most people. However there is a convention in mathematical physics to define new units for every

particular problem and write formulas in terms of these new units. This process is often called normalization. This has the advantage of possibly reducing the numbe of free parameters in a prolem. Another advantage is that, by chosen proper characteristic quantites as units, the magnitude of quanties in terms of the new units are easier to be appreciated. A third advantage, which is usually not important, is that the magnitude of normalized quantities may be in the vicinity of 1 and thus avoid possible numerical overflow in a numerical computionation.

The disadvantages of the normalization are the additional work associated with performing the transformation between the two units systems and possible confusions associated with the exact units used in a numerical code and the potential of introducing bugs due to this confusion when writing numerical codes.

Choose a characteristic magnetic field strength B_n and a characteristic length L_n. Using B_n and L_n, we define a characteristic time $t_n \equiv 2\pi / \Omega_n$, where $\Omega_n = B_n|Ze|/m$, a characteristic velocity $v_n = L_n / t_n$, and a characteristic magnetic moment $\mu_n = m v_n^2 / B_n$. Using these characteristic quantities as units, we define the following normalized quantities in terms of the new units:

$$\overline{\mathbf{X}} = \frac{\mathbf{X}}{L_n}, \overline{\nabla} = L_n \nabla, \bar{t} = \frac{t}{t_n}, \overline{v}_\parallel = \frac{v_\parallel}{v_n}, \overline{\mu} = \frac{\mu}{\mu_n}, \overline{\mathbf{B}} = \frac{\mathbf{B}}{B_n}, \overline{\mathbf{B}^\star} = \frac{\mathbf{B}^\star}{B_n}, \overline{B_\parallel^\star} = \frac{B_\parallel^\star}{B_n}, \overline{\mathbf{E}} = \frac{\mathbf{E}}{B_n v_n}. \tag{8}$$

In terms of the above normalized quantities, Eqs. (1)-(4) are written, respectively, as

$$\frac{d\overline{\mathbf{X}}}{d\,\bar{t}} = \overline{\mathbf{v}}_d = \frac{\overline{\mathbf{B}^\star}}{\overline{B_\parallel^\star}}\overline{v}_\parallel + \frac{Z}{|Z|}\frac{\overline{\mu}}{2\pi\,\overline{B}\,\overline{B_\parallel^\star}}\overline{\mathbf{B}} \times \overline{\nabla}\overline{B} + \frac{1}{\overline{B}\,\overline{B_\parallel^\star}}\overline{\mathbf{E}} \times \overline{\mathbf{B}}, \tag{9}$$

$$\frac{d\,\overline{v}_\parallel}{d\,\bar{t}} = -\overline{\mu}\frac{\overline{\mathbf{B}^\star}}{\overline{B_\parallel^\star}} \cdot \overline{\nabla}\overline{B} + \frac{Z}{|Z|} 2\pi \frac{\mathbf{B}^\star}{B_\parallel^\star} \cdot \overline{\mathbf{E}}, \tag{10}$$

$$\overline{\mathbf{B}^\star} = \overline{\mathbf{B}} + \frac{Z}{|Z|}\frac{\overline{v}_\parallel}{2\pi}\overline{\nabla} \times \mathbf{b}, \tag{11}$$

and

$$\overline{B_\parallel^\star} = \overline{B}\left(1 + \frac{Z}{|Z|}\frac{\overline{v}_\parallel}{2\pi\overline{B}}\mathbf{b} \cdot \overline{\nabla} \times \mathbf{b}\right). \tag{12}$$

In the normalized form, there is only one parameter for distinguishing particle species, namely the sign of particle's charge $Z/|Z|$. The other parameters for particle species enters via $\Omega_n = B_n|Ze|/m$.

1.2 Equation of guding-center motion in field-line-following coordinates

This section documents what I did when developing the fully kinetic ions and drift-kinetic electrons module in GEM code which uses field-line-folloiwng coordinates. In field-line-following coordinates (ψ, θ, α), the equation of guiding-center drift is written as

$$\frac{d\,\psi}{d\,\bar{t}} = \overline{\mathbf{v}}_d \cdot \overline{\nabla}\,\psi, \tag{13}$$

$$\frac{d\,\theta}{d\,\bar{t}} = \overline{\mathbf{v}}_d \cdot \overline{\nabla}\,\theta, \tag{14}$$

$$\frac{d\,\alpha}{d\,\bar{t}} = \overline{\mathbf{v}}_d \cdot \overline{\nabla}\,\alpha, \tag{15}$$

where α is the generalized toroidal angle defined by (refer to my notes on tokamak equilibrium) $\alpha = \phi - \bar{\delta}$ with $\bar{\delta} = \int_0^\theta \hat{q} d\theta$ and $\hat{q} = \mathbf{B} \cdot \nabla\phi / (\mathbf{B} \cdot \nabla\theta)$, which is the local safety factor. Using the expression of $\overline{\mathbf{v}}_d$ given by Eq. (9), the right-hand-sides of Eqs. (13)-(15) to can be written as (presently dropping the $\mathbf{E} \times \mathbf{B}$ drift):

$$\overline{\mathbf{v}}_d \cdot \overline{\nabla}\,\psi = \overline{v}_\parallel \frac{\frac{Z}{|Z|}\frac{\overline{v}_\parallel}{2\pi}\overline{\nabla} \times \mathbf{b}}{\overline{B}\left(1 + \frac{Z}{|Z|}\frac{\overline{v}_\parallel}{2\pi\overline{B}}\mathbf{b} \cdot \overline{\nabla} \times \mathbf{b}\right)} \cdot \overline{\nabla}\,\psi + \frac{Z}{|Z|}\frac{\overline{\mu}}{2\pi\left(1 + \frac{Z}{|Z|}\frac{\overline{v}_\parallel}{2\pi\overline{B}}\mathbf{b} \cdot \overline{\nabla} \times \mathbf{b}\right)}\frac{1}{\overline{B}^2}\overline{\mathbf{B}} \times \overline{\nabla}\overline{B} \cdot \overline{\nabla}\,\psi, \tag{16}$$

$$\overline{\mathbf{v}}_d \cdot \overline{\nabla}\,\theta = \overline{v}_\parallel \frac{\overline{\mathbf{B}} + \frac{Z}{|Z|}\frac{\overline{v}_\parallel}{2\pi}\overline{\nabla} \times \mathbf{b}}{\overline{B}\left(1 + \frac{Z}{|Z|}\frac{\overline{v}_\parallel}{2\pi\overline{B}}\mathbf{b} \cdot \overline{\nabla} \times \mathbf{b}\right)} \cdot \overline{\nabla}\,\theta + \frac{Z}{|Z|}\frac{\overline{\mu}}{2\pi\left(1 + \frac{Z}{|Z|}\frac{\overline{v}_\parallel}{2\pi\overline{B}}\mathbf{b} \cdot \overline{\nabla} \times \mathbf{b}\right)}\frac{1}{\overline{B}^2}\overline{\mathbf{B}} \times \overline{\nabla}\overline{B} \cdot \overline{\nabla}\,\theta, \tag{17}$$

$$\overline{\mathbf{v}}_d\cdot\overline{\nabla}\,\alpha \;=\; \overline{v}_\parallel\frac{\frac{Z}{|Z|}\frac{\overline{v}_\parallel}{2\pi}\overline{\nabla}\times\mathbf{b}}{\overline{B}\Big(1+\frac{Z}{|Z|}\frac{\overline{v}_\parallel}{2\pi\overline{B}}\mathbf{b}\cdot\overline{\nabla}\times\mathbf{b}\Big)}\cdot\overline{\nabla}\,\alpha+\frac{Z}{|Z|}\frac{\overline{\mu}}{2\pi\left(1+\frac{Z}{|Z|}\frac{\overline{v}_\parallel}{2\pi\overline{B}}\mathbf{b}\cdot\overline{\nabla}\times\mathbf{b}\right)}\frac{1}{\overline{B}^2}\overline{\mathbf{B}}\times\overline{\nabla}\overline{B}\cdot\overline{\nabla}\,\alpha. \tag{18}$$

where use has been made of $\mathbf{B}\cdot\nabla\psi=0$ and $\mathbf{B}\cdot\nabla\alpha=0$. The parallel acceleration equation is written as (presently dropping the electric field acceleration term)

$$\frac{d\,\overline{v}_\parallel}{d\,\overline{t}}=-\overline{\mu}\frac{\overline{\mathbf{B}}+\frac{Z}{|Z|}\frac{\overline{v}_\parallel}{2\pi}\overline{\nabla}\times\mathbf{b}}{\overline{B}\Big(1+\frac{Z}{|Z|}\frac{\overline{v}_\parallel}{2\pi\overline{B}}\mathbf{b}\cdot\overline{\nabla}\times\mathbf{b}\Big)}\cdot\overline{\nabla}\overline{B} \tag{19}$$

For a general tokamak magnetic configuration specifed numerically, all the above 2D equilibrium quantitis are computed by interpolating pre-computed numerical tables. We define the following numerical tables:

$$W_1(\psi,\theta)=\frac{1}{\overline{B}}\mathbf{b}\cdot\overline{\nabla}\times\mathbf{b}, \tag{20}$$

$$W_2(\psi,\theta)=\frac{\overline{\mathbf{B}}}{\overline{B}}\cdot\overline{\nabla}\,\theta, \tag{21}$$

$$W_3(\psi,\theta)=\frac{\overline{\nabla}\times\mathbf{b}}{\overline{B}}\cdot\overline{\nabla}\,\psi, \tag{22}$$

$$W_4(\psi,\theta)=\frac{\overline{\nabla}\times\mathbf{b}}{\overline{B}}\cdot\overline{\nabla}\,\theta, \tag{23}$$

$$W_5(\psi,\theta,\alpha)=\frac{\overline{\nabla}\times\mathbf{b}}{\overline{B}}\cdot\overline{\nabla}\,\alpha=\frac{\overline{\nabla}\times\mathbf{b}}{\overline{B}}\cdot\overline{\nabla}\,\phi-\frac{\overline{\nabla}\times\mathbf{b}}{\overline{B}}\cdot\overline{\nabla}\delta \tag{24}$$

$$W_6(\psi,\theta)=\frac{1}{\overline{B}^2}\overline{\mathbf{B}}\times\overline{\nabla}\overline{B}\cdot\overline{\nabla}\,\psi, \tag{25}$$

$$W_7(\psi,\theta)=\frac{1}{\overline{B}^2}\overline{\mathbf{B}}\times\overline{\nabla}\overline{B}\cdot\overline{\nabla}\,\theta, \tag{26}$$

$$W_8(\psi,\theta,\alpha)=\frac{1}{\overline{B}^2}\overline{\mathbf{B}}\times\overline{\nabla}\overline{B}\cdot\overline{\nabla}\,\alpha=\frac{1}{\overline{B}^2}\overline{\mathbf{B}}\times\overline{\nabla}\overline{B}\cdot\overline{\nabla}\,\phi-\frac{1}{\overline{B}^2}\overline{\mathbf{B}}\times\overline{\nabla}\overline{B}\cdot\overline{\nabla}\delta \tag{27}$$

$$W_9(\psi,\theta)=\frac{\overline{\mathbf{B}}}{\overline{B}}\cdot\overline{\nabla}\overline{B}, \tag{28}$$

$$W_{10}(\psi,\theta)=\frac{\overline{\nabla}\times\mathbf{b}}{\overline{B}}\cdot\overline{\nabla}\overline{B}. \tag{29}$$

Next, let us disscuss the $E\times B$ drift:

$$\overline{\mathbf{v}}_{E\times B}\cdot\nabla\psi=\frac{1}{\overline{B}\,\overline{B}^\star_\parallel}\overline{\mathbf{E}}\times\overline{\mathbf{B}}\cdot\overline{\nabla}\,\psi \tag{30}$$

$$\overline{\mathbf{v}}_{E\times B}\cdot\nabla\theta=\frac{1}{\overline{B}\,\overline{B}^\star_\parallel}\overline{\mathbf{E}}\times\overline{\mathbf{B}}\cdot\overline{\nabla}\,\theta \tag{31}$$

$$\overline{\mathbf{v}}_{E\times B}\cdot\nabla\alpha=\frac{1}{\overline{B}\,\overline{B}^\star_\parallel}\overline{\mathbf{E}}\times\overline{\mathbf{B}}\cdot\overline{\nabla}\,\alpha \tag{32}$$

Using $\delta\overline{\mathbf{E}}=\delta\overline{E}_\parallel\mathbf{b}+\delta\overline{E}_x\overline{\nabla}x+\delta\overline{E}_y\overline{\nabla}y$, the above drifts are written as

$$\begin{aligned}\overline{\mathbf{v}}_{E\times B}\cdot\nabla x \;&=\; \frac{1}{\overline{B}\,\overline{B}^\star_\parallel}(\delta\overline{E}_x\overline{\nabla}x+\delta\overline{E}_y\overline{\nabla}y)\times\overline{\mathbf{B}}\cdot\overline{\nabla}\,x\\ &=\; -\frac{1}{\overline{B}\,\overline{B}^\star_\parallel}(\delta\overline{E}_x\overline{\nabla}x+\delta\overline{E}_y\overline{\nabla}y)\times\overline{\nabla}\,x\cdot\overline{\mathbf{B}}\end{aligned}$$

$$
\begin{aligned}
&= -\frac{1}{\overline{B}\,\overline{B}^{\star}_{\parallel}}(\delta\overline{E}_y\overline{\nabla}y)\times\overline{\nabla}\,x\cdot\overline{\mathbf{B}}\\
&= \frac{1}{\overline{B}\,\overline{B}^{\star}_{\parallel}}(\delta\overline{E}_y)\overline{\nabla}x\times\overline{\nabla}\,y\cdot\overline{\mathbf{B}}\\
&= \frac{1}{\overline{B}\,\overline{B}^{\star}_{\parallel}}(\delta\overline{E}_y)\frac{\overline{\mathbf{B}}}{\overline{\Psi}'}\cdot\overline{\mathbf{B}} \qquad (33)
\end{aligned}
$$

$$
\begin{aligned}
\overline{\mathbf{v}}_{E\times B}\cdot\nabla y &= \frac{1}{\overline{B}\,\overline{B}^{\star}_{\parallel}}(\delta\overline{E}_x\overline{\nabla}x+\delta\overline{E}_y\overline{\nabla}y)\times\overline{\mathbf{B}}\cdot\overline{\nabla}\,y\\
&= -\frac{1}{\overline{B}\,\overline{B}^{\star}_{\parallel}}(\delta\overline{E}_x\overline{\nabla}x+\delta\overline{E}_y\overline{\nabla}y)\times\overline{\nabla}\,y\cdot\overline{\mathbf{B}}\\
&= -\frac{1}{\overline{B}\,\overline{B}^{\star}_{\parallel}}(\delta\overline{E}_x\overline{\nabla}x)\times\overline{\nabla}\,y\cdot\overline{\mathbf{B}}\\
&= -\frac{1}{\overline{B}\,\overline{B}^{\star}_{\parallel}}(\delta\overline{E}_x)\frac{\overline{\mathbf{B}}}{\overline{\Psi}'}\cdot\overline{\mathbf{B}} \qquad (34)
\end{aligned}
$$

$$
\begin{aligned}
\overline{\mathbf{v}}_{E\times B}\cdot\nabla\theta &= \frac{1}{\overline{B}\,\overline{B}^{\star}_{\parallel}}(\delta\overline{E}_x\overline{\nabla}\psi+\delta\overline{E}_y\overline{\nabla}\alpha)\times\overline{\mathbf{B}}\cdot\overline{\nabla}\,\theta\\
&= -\frac{1}{\overline{B}\,\overline{B}^{\star}_{\parallel}}(\delta\overline{E}_x\overline{\mathbf{B}}\cdot\overline{\nabla}\psi\times\overline{\nabla}\,\theta+\delta\overline{E}_y\overline{\mathbf{B}}\cdot\overline{\nabla}\alpha\times\overline{\nabla}\,\theta). \qquad (35)
\end{aligned}
$$

The two terms in expression (35) and be written as

$$
\overline{\mathbf{B}}\cdot(\overline{\nabla}\psi\times\overline{\nabla}\,\theta)=\overline{\mathbf{B}}\cdot\begin{vmatrix}\mathbf{e}_R & \mathbf{e}_\phi & \mathbf{e}_Z\\ \frac{\partial\psi}{\partial R} & 0 & \frac{\partial\psi}{\partial Z}\\ \frac{\partial\theta}{\partial R} & 0 & \frac{\partial\theta}{\partial Z}\end{vmatrix}=\overline{B}_\phi\left(\frac{\partial\psi}{\partial Z}\frac{\partial\theta}{\partial R}-\frac{\partial\psi}{\partial R}\frac{\partial\theta}{\partial Z}\right)\equiv W_{14} \qquad (36)
$$

$$
\overline{\mathbf{B}}\cdot(\overline{\nabla}\alpha\times\overline{\nabla}\,\theta)=\overline{\mathbf{B}}\cdot\begin{vmatrix}\mathbf{e}_R & \mathbf{e}_\phi & \mathbf{e}_Z\\ \frac{\partial\alpha}{\partial R} & \frac{1}{R}\frac{\partial\alpha}{\partial\phi} & \frac{\partial\alpha}{\partial Z}\\ \frac{\partial\theta}{\partial R} & 0 & \frac{\partial\theta}{\partial Z}\end{vmatrix}=\overline{B}_R\left(\frac{1}{R}\frac{\partial\alpha}{\partial\phi}\frac{\partial\theta}{\partial Z}\right)+\overline{B}_\phi\left(\frac{\partial\alpha}{\partial Z}\frac{\partial\theta}{\partial R}-\frac{\partial\alpha}{\partial R}\frac{\partial\theta}{\partial Z}\right)+\overline{B}_Z\left(-\frac{1}{R}\frac{\partial\alpha}{\partial\phi}\frac{\partial\theta}{\partial R}\right)\equiv W_{15} \qquad (37)
$$

1.2.1 Periodic conditions of particle trajactory in field-line-following coordinates

Note that $\theta(\mathbf{r})$ and $\phi(\mathbf{r})$ are multi-valued functions, while $\nabla\theta(\mathbf{r})$ and $\nabla\phi(\mathbf{r})$ happens to be a single-valued function. However $\nabla\alpha(\mathbf{r})$ and $\nabla\overline{\delta}(\mathbf{r})$ are still multi-valued functions. [It is ready to see this point by examing the special case that θ is a straight-field line poloidal angle, in which $\int_0^\theta\hat{q}d\theta$ is simplified to $q\theta$. Then $\nabla\overline{\delta}$ is written as

$$
\nabla\overline{\delta}=\theta\nabla q+q\nabla\theta, \qquad (38)
$$

where the first term $\theta\nabla q$ is a multi-valued function since θ is multi-valued.] For multi-valued functions, if a single branch is chosen, then there will be discontinuity at the the branch cut.

In numerically constructing the coordinates (ψ,θ,α), the principal value of θ is chosen in the range $[-\pi\colon\pi]$ and the branch cut for θ is chosen on the high-field-side midplane. The toroidal shift $\overline{\delta}=\int_0^\theta\hat{q}\,d\,\theta$ can be considered as a derived angle based on θ and thus its principal value and branch cut are determined by those of θ. Specificly, the principal value of $\overline{\delta}$ is in the range $[-\pi q\colon\pi q]$ for up-down symmetrical equilibria and the branch cut is also on the high-field-side midplane.

The (ψ,θ,α) coordinates of a particle change continously when they are evolved by using Eqs. (13)-(15), during which θ can move beyond $[-\pi,\pi]$. When a particle's θ moves beyong the range $[-\pi\colon\pi]$, one or multiple $\pm2\pi$ shifts are imposed on θ until θ are within $[-\pi\colon\pi]$. Note that a cooresponding shift in α is needed to keep the particle at the same spatial location when doing the θ shift. This is because, although (ψ,θ,ϕ) and $(\psi,\theta-2\pi,\phi)$ correspond to the same spatial location, points (ψ,θ,α) and $(\psi,\theta-2\pi,\alpha)$ do not. Specificly, the usual toroidal angle ϕ of point (ψ,θ,α) is $\phi_1=\alpha+\int_0^\theta\hat{q}d\theta$ while ϕ of point $(\psi,\theta-2\pi,\alpha)$ is $\phi_2=\alpha+\int_0^{\theta-2\pi}\hat{q}d\theta$. The difference between ϕ_1 and ϕ_2 is $\phi_2-\phi_1=-2\pi q$. This indicates that, to keep the point at the same spatial location when shifting θ by -2π, α should be shifted by $+2\pi q$, i.e., the new coordinates of the point should be $(\psi,\theta-2\pi,\alpha+2\pi q)$. This process is illustrated in Fig. 1 and a typical evolution of (θ,α) involving shifting is shown in Fig. (2).

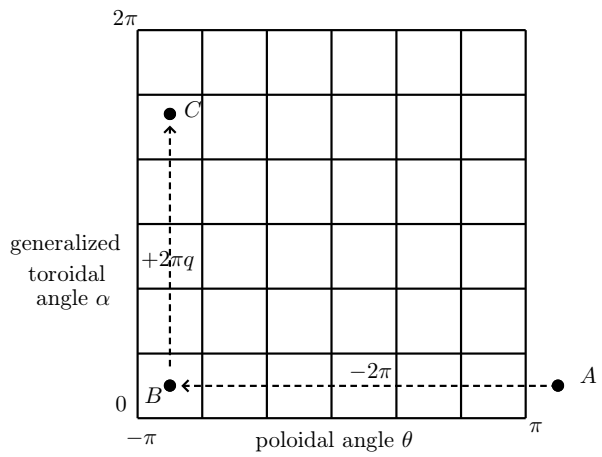

Figure 1. To keep the point at the same spatial location when shifting θ by -2π, α should be shifted by $+2\pi q$. Here A and C correspond to the same spatial location, but B is at a different location.

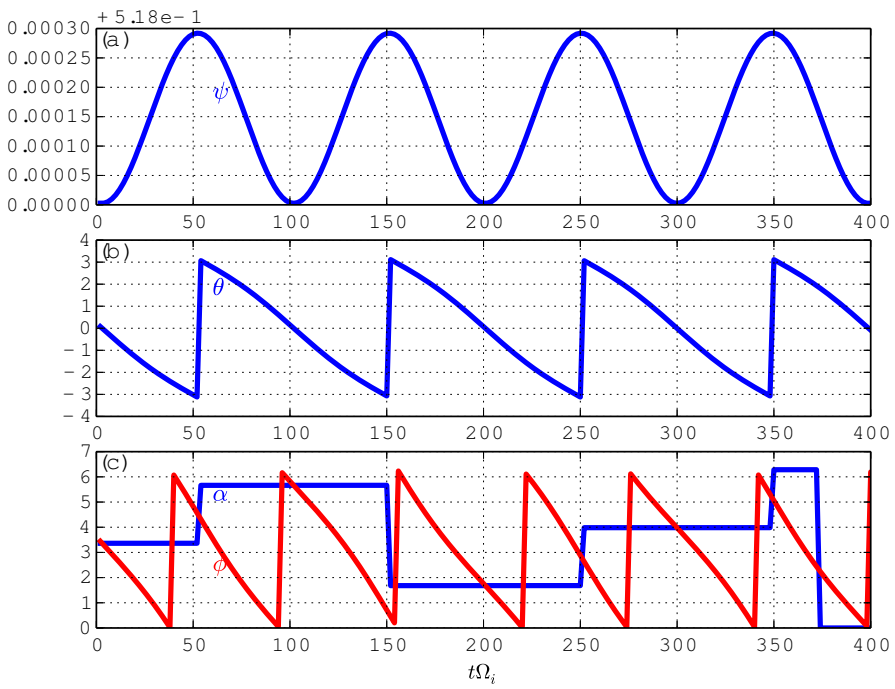

Figure 2. Temporal evolution of (ψ, θ, α) of a passing electron. The range of θ is chosen to be $[-\pi\colon \pi]$ and the range of α and ϕ is $[0\colon 2\pi]$. When θ exeed the range, a 2π shift is imposed, which generate the jump of θ in (b) and also the corresponding jump of α in (c). Note that when a jump in (θ, α) ocurs, no jump in ϕ, which is what we expect, otherwise there must be something wrong. Also note that there are also jumps of ϕ shown in (c), which is due to ϕ exceeding the range $[0\colon 2\pi]$ and a 2π shift being imposed and this jump has nothing to do with the jump in θ or α and usually occur at different time (one jump of ϕ is near the jump of α, which is only a coincidence). Here ϕ is computed using $\phi = \alpha + \bar{\delta}$, where $\bar{\delta}$ is obtained by interpolating the 2D numerical table of $\bar{\delta}(\psi, \theta)$. DIID-D cyclone base case

(When α of a particle moves beyong the range $[0\colon 2\pi]$, one or multiple $\pm 2\pi$ shifts are imposed on α until α are within $[0\colon 2\pi]$. Since, for fixed ψ and θ, the generalized toroidal angle α is equivalent to the usual toroidal angle ϕ. No complication like the case of θ arises when doing the α shift.)

One way of avoiding the subtle (θ, α) shift problem is to evolve particles' ϕ, instead of α. In this case, we have

$$\frac{d\,\phi}{d\,\overline{t}} = \overline{\mathbf{v}}_d \cdot \overline{\nabla}\,\phi \;=\; \overline{v}_{\parallel} \frac{\overline{\mathbf{B}} + \frac{\overline{v}_{\parallel}}{2\pi}\overline{\nabla}\times\mathbf{b}}{\overline{B}\left(1 + \frac{\overline{v}_{\parallel}}{2\pi\overline{B}}\mathbf{b}\cdot\overline{\nabla}\times\mathbf{b}\right)} \cdot \overline{\nabla}\,\phi + \frac{\overline{\mu}}{2\pi\left(1 + \frac{\overline{v}_{\parallel}}{2\pi\overline{B}}\mathbf{b}\cdot\overline{\nabla}\times\mathbf{b}\right)} \frac{1}{\overline{B}^2}\overline{\mathbf{B}}\times\overline{\nabla}\overline{B}\cdot\overline{\nabla}\,\phi, \tag{39}$$

After geting ϕ, we use $\alpha = \phi - \bar{\delta}(\psi, \theta)$ to get particles' α, where $\bar{\delta}$ is obtained by interpolating the numerical table in (ψ, θ) plane. I have tested the two ways of computing evolution of α, which indicates their results agree with each other. In the final codes, I use the (θ, α) shift method, because this methods involve less interpolation and

thus more efficient.

1.2.2 Benchmarking cases

To verify code implementation, two methods are used to compute the guiding-center orbits. The first method uses the cylindrical coordinates and then interpolate the orbits into magnetic coordinates using pre-computed mapping table between the cylindrical and magnetic coordinates. The second method directly uses the magnetic coordinates in pushing the orbits. The following figures compare the results obtained by these two methods, which indicates they agree with each other. This provdies confidence on the correctness of the numerical implementation.

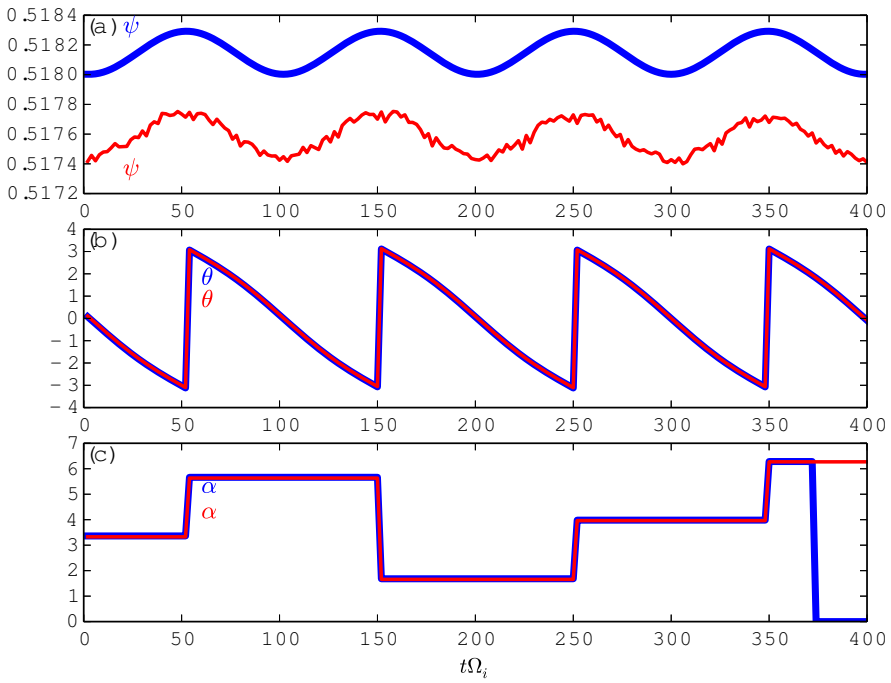

Figure 3. Comparison between the temporal evolution of (ψ, θ, α) of a passing electron computed by two methods: the blue lines are the results computed directly in (ψ, θ, α) field-line-following coordinates, the red lines are results computed in cylindrical coordinates and then interpolated to the field-line-following coordinates. There is sysmetical discrepancy between ψ computed by the two methods. The results are actually very close to each other and the differebce becomes obvious because the variation of ψ is very small for a passing electron.

The results of α from the two methods also agree with each other. The discrepancy near $t\Omega_i = 400$ is due to that α is close to 2π, and one result becomes zero, which is equivalent to 2π.

equilibrium is the DIID-D cyclone base case

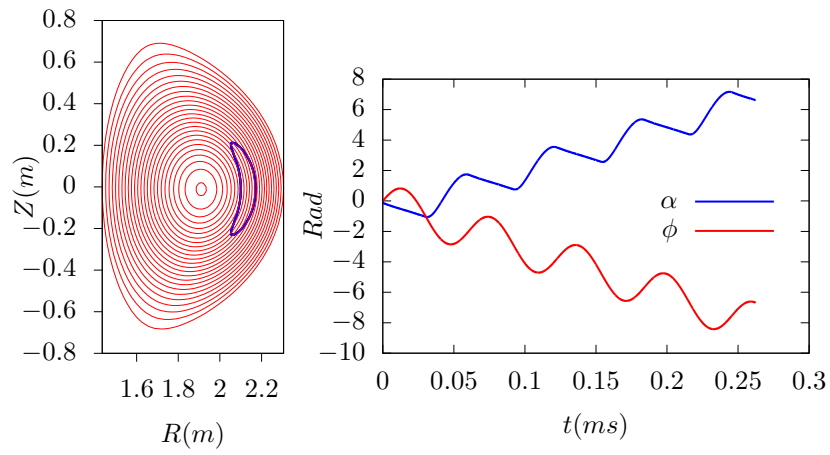

Figure 4. Left: orbit on poloidal plane. Right: α is defined by $\alpha = \phi - \int_0^\theta \hat{q} d\,\theta$, where ϕ is the usual cylindrical toroidal angle.

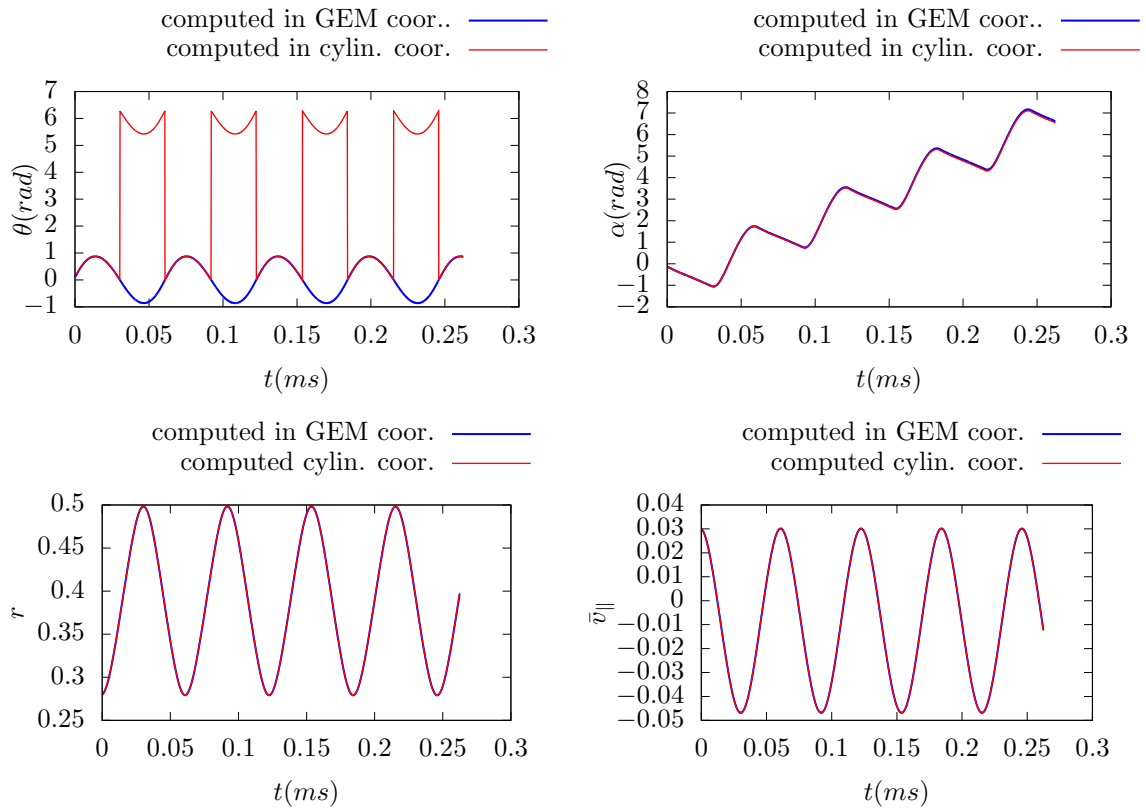

Figure 5. The evolutions of the poloidal angles θ and generalized toroidal anglecal α culated by the two methods agree with each other. $r = \sqrt{\frac{\Psi - \Psi_0}{\Psi_b - \Psi_0}}$

1.3 Equations of guiding-center motion in cylindrical coordinates

In this section, all quantities are in the normalized form given in Sec. 1.1. For notational simplicity, the overbars of the notation are ommitted. In cylindrical coordinates $(R,\, \phi,\, Z)$, the location vector is written as $\mathbf{X} = R\hat{\mathbf{e}}_R + Z\hat{\mathbf{e}}_Z$. Using this, we obtain

$$\frac{d\mathbf{X}}{dt} = \frac{dR}{dt}\hat{\mathbf{e}}_R + R\frac{d\phi}{dt}\hat{\mathbf{e}}_\phi + \frac{dZ}{dt}\hat{\mathbf{e}}_Z \tag{40}$$

Substituting this into Eq. (1) gives

$$\frac{dR}{dt}\hat{\mathbf{e}}_R + R\frac{d\phi}{dt}\hat{\mathbf{e}}_\phi + \frac{dZ}{dt}\hat{\mathbf{e}}_Z = \frac{\mathbf{B}^\star}{B^\star_\|}v_\| + \frac{\mu}{2\pi B B^\star}\mathbf{B}\times\nabla B + \frac{1}{BB^\star_\|}\mathbf{E}\times\mathbf{B}, \tag{41}$$

from which we obtain the following component equations:

$$\frac{dR}{dt} = \left[\frac{\mathbf{B}^\star}{B^\star_\|}v_\| + \frac{\mu}{2\pi B B^\star_\|}\mathbf{B}\times\nabla B + \frac{1}{BB^\star_\|}\mathbf{E}\times\mathbf{B}\right]\cdot\hat{\mathbf{e}}_R \tag{42}$$

$$\frac{dZ}{dt} = \left[\frac{\mathbf{B}^\star}{B^\star_\|}v_\| + \frac{\mu}{2\pi B B^\star_\|}\mathbf{B}\times\nabla B + \frac{1}{BB^\star_\|}\mathbf{E}\times\mathbf{B}\right]\cdot\hat{\mathbf{e}}_Z, \tag{43}$$

$$\frac{d\phi}{dt} = \frac{1}{R}\left[\frac{\mathbf{B}^\star}{B^\star_\|}v_\| + \frac{\mu}{2\pi B B^\star_\|}\mathbf{B}\times\nabla B + \frac{1}{BB^\star_\|}\mathbf{E}\times\mathbf{B}\right]\cdot\hat{\mathbf{e}}_\phi, \tag{44}$$

In the cylindrical coordinates, the terms $\nabla\times\mathbf{b}$, $\mathbf{b}\cdot\nabla\times\mathbf{b}$, and $\mathbf{B}\times\nabla B$ can be written, respectively, as

$$\nabla\times\mathbf{b} = \left(\frac{1}{R}\frac{\partial b_Z}{\partial\phi} - \frac{\partial b_\phi}{\partial z}\right)\hat{e}_R + \left(\frac{\partial b_R}{\partial Z} - \frac{\partial b_Z}{\partial R}\right)\hat{e}_\phi + \left(\frac{1}{R}\frac{\partial(Rb_\phi)}{\partial R} - \frac{1}{R}\frac{\partial b_R}{\partial\phi}\right)\hat{e}_Z \tag{45}$$

$$\mathbf{b}\cdot\nabla\times\mathbf{b} = b_R\left(\frac{1}{R}\frac{\partial b_Z}{\partial\phi} - \frac{\partial b_\phi}{\partial z}\right) + b_\phi\left(\frac{\partial b_R}{\partial Z} - \frac{\partial b_Z}{\partial R}\right) + b_Z\left(\frac{1}{R}\frac{\partial(Rb_\phi)}{\partial R} - \frac{1}{R}\frac{\partial b_R}{\partial\phi}\right). \tag{46}$$

$$\mathbf{B}\times\nabla B = \begin{vmatrix} \hat{e}_R & \hat{e}_\phi & \hat{e}_Z \\ B_R & B_\phi & B_Z \\ \frac{\partial B}{\partial R} & \frac{1}{R}\frac{\partial B}{\partial\phi} & \frac{\partial B}{\partial Z} \end{vmatrix} \tag{47}$$

Using $b_R = \frac{B_R}{B}$, $b_Z = \frac{B_Z}{B}$, and $b_\phi = \frac{B_\phi}{B}$, we obtain

$$\begin{cases} \frac{\partial b_R}{\partial R} = \frac{\frac{\partial B_R}{\partial R}B - \frac{\partial B}{\partial R}B_R}{B^2} \\ \frac{\partial b_R}{\partial Z} = \frac{\frac{\partial B_R}{\partial Z}B - \frac{\partial B}{\partial Z}B_R}{B^2} \\ \frac{\partial b_R}{\partial \phi} = \frac{\frac{\partial B_R}{\partial \phi}B - \frac{\partial B}{\partial \phi}B_R}{B^2} \end{cases} \quad \begin{cases} \frac{\partial b_Z}{\partial R} = \frac{\frac{\partial B_Z}{\partial R}B - \frac{\partial B}{\partial R}B_Z}{B^2} \\ \frac{\partial b_Z}{\partial Z} = \frac{\frac{\partial B_Z}{\partial Z}B - \frac{\partial B}{\partial Z}B_Z}{B^2} \\ \frac{\partial b_Z}{\partial \phi} = \frac{\frac{\partial B_Z}{\partial \phi}B - \frac{\partial B}{\partial \phi}B_Z}{B^2} \end{cases} \quad \begin{cases} \frac{\partial b_\phi}{\partial R} = \frac{\frac{\partial B_\phi}{\partial R}B - \frac{\partial B}{\partial R}B_\phi}{B^2} \\ \frac{\partial b_\phi}{\partial Z} = \frac{\frac{\partial B_\phi}{\partial Z}B - \frac{\partial B}{\partial Z}B_\phi}{B^2} \\ \frac{\partial b_\phi}{\partial \phi} = \frac{\frac{\partial B_\phi}{\partial \phi}B - \frac{\partial B}{\partial \phi}B_\phi}{B^2} \end{cases} \tag{48}$$

The equation for $v_\parallel$ is given by

$$\frac{dv_\parallel}{dt} = -\mu \frac{\mathbf{B}^\star}{B_\parallel^\star} \cdot \nabla B + 2\pi \frac{\mathbf{B}^\star}{B_\parallel^\star} \cdot \mathbf{E}. \tag{49}$$

The first term on the left-hand-side of the above equation is written

$$\frac{\mathbf{B}^\star}{B_\parallel^\star} \cdot \nabla B = \frac{B_R^\star}{B_\parallel^\star}\frac{\partial B}{\partial R} + \frac{B_\phi^\star}{B_\parallel^\star}\frac{1}{R}\frac{\partial B}{\partial \phi} + \frac{B_Z^\star}{B_\parallel^\star}\frac{\partial B}{\partial Z} \tag{50}$$

$$B_R^\star = B_R + \frac{v_\parallel}{2\pi}\left(\frac{1}{R}\frac{\partial b_Z}{\partial \phi} - \frac{\partial b_\phi}{\partial z}\right) \tag{51}$$

$$B_Z^\star = B_Z + \frac{v_\parallel}{2\pi}\left(\frac{1}{R}\frac{\partial (R b_\phi)}{\partial R} - \frac{1}{R}\frac{\partial b_R}{\partial \phi}\right) \tag{52}$$

$$B_\phi^\star = B_\phi + \frac{v_\parallel}{2\pi}\left(\frac{\partial b_R}{\partial Z} - \frac{\partial b_Z}{\partial R}\right) \tag{53}$$

1.4 Equilibrium magnetic field in tokamak

The tokamak equilbrium magnetic field can be written

$$\mathbf{B} = \nabla\Psi \times \nabla\phi + g(\Psi)\nabla\phi. \tag{54}$$

In my code, the values of the two free functions, $\Psi = \Psi(R, Z)$ and $g(\Psi)$, which sepcify the magnetic field, is read from the output file "G-eqdsk-file" of EFIT code. Using Eq. (54), the axisymmetric equilibrium magnetic field can be written as

$$B_R = -\frac{1}{R}\frac{\partial \Psi}{\partial Z}, \tag{55}$$

$$B_Z = \frac{1}{R}\frac{\partial \Psi}{\partial R}, \tag{56}$$

$$B_\phi = \frac{g(\Psi)}{R}. \tag{57}$$

The partial derivative of the component of the magnetic field is written as

$$\frac{\partial B_R}{\partial R} = \frac{1}{R^2}\frac{\partial \Psi}{\partial Z} - \frac{1}{R}\frac{\partial^2 \Psi}{\partial Z \partial R} \tag{58}$$

$$\frac{\partial B_R}{\partial Z} = -\frac{1}{R}\frac{\partial^2 \Psi}{\partial Z^2} \tag{59}$$

$$\frac{\partial B_Z}{\partial R} = -\frac{1}{R^2}\frac{\partial \Psi}{\partial R} + \frac{1}{R}\frac{\partial^2 \Psi}{\partial R^2} \tag{60}$$

$$\frac{\partial B_Z}{\partial Z} = \frac{1}{R}\frac{\partial^2 \Psi}{\partial R \partial Z} \tag{61}$$

$$\frac{\partial B_\phi}{\partial R} = -\frac{1}{R^2}g(\Psi) + \frac{1}{R}g'(\Psi)\frac{\partial \Psi}{\partial R} \tag{62}$$

$$\frac{\partial B_\phi}{\partial Z} = \frac{1}{R}g'(\Psi)\frac{\partial \Psi}{\partial Z} \tag{63}$$

$$\Rightarrow B = \frac{1}{R}\sqrt{\left(\frac{\partial \Psi}{\partial R}\right)^2 + \left(\frac{\partial \Psi}{\partial Z}\right)^2 + g^2} \tag{64}$$

$$\begin{aligned} \frac{\partial B}{\partial R} &= -\frac{1}{R^2}BR + \frac{1}{R}\frac{1}{2}\frac{1}{BR}\left(2\frac{\partial \Psi}{\partial R}\frac{\partial^2 \Psi}{\partial R^2} + 2\frac{\partial \Psi}{\partial Z}\frac{\partial^2 \Psi}{\partial Z \partial R} + 2g\frac{\partial g}{\partial R}\right) \\ &= -\frac{B}{R} + \frac{1}{BR^2}\left(\frac{\partial \Psi}{\partial R}\frac{\partial^2 \Psi}{\partial R^2} + \frac{\partial \Psi}{\partial Z}\frac{\partial^2 \Psi}{\partial Z \partial R} + g\frac{\partial g}{\partial R}\right) \end{aligned} \tag{65}$$

$$\frac{\partial B}{\partial Z} = \frac{1}{R}\frac{1}{2}\frac{1}{BR}\left(2\frac{\partial\Psi}{\partial R}\frac{\partial^2\Psi}{\partial R\partial Z}+2\frac{\partial\Psi}{\partial Z}\frac{\partial^2\Psi}{\partial Z^2}+2g\frac{\partial g}{\partial Z}\right)$$
$$= \frac{1}{BR^2}\left(\frac{\partial\Psi}{\partial R}\frac{\partial^2\Psi}{\partial R\partial Z}+\frac{\partial\Psi}{\partial Z}\frac{\partial^2\Psi}{\partial Z^2}+g\frac{\partial g}{\partial Z}\right) \quad (66)$$

In my numerical code, the numerical data of the poloidal flux function $\Psi(R,Z)$ and toroidal field function $g(\Psi)$ are read in from the output G-eqdsk file of the EFIT code. Then all the partial derivatives are calculated by using central finite-difference. Then the linear interpolation is used to evaluate the various quantities that are needed at the instantenous location of guiding-centers to push the orbits.

1.4.1 Solovév equilibrium

When I began to write the guiding center orbit code, in order to avoid the numerical interpolating, I use Solovev's analytic equilibrium. (The latest version of my code constructs magnetic field by reading the output G-eqdsk file of the EFIT code and thus can treat general tokamak magnetic field.) The Solovév equilibrium is an analytic equilibrium in which the poloidal flux function Ψ is given by

$$\Psi = \frac{B_0}{2R_0^2\kappa_0 q_0}\left[R^2Z^2+\frac{\kappa_0^2}{4}(R^2-R_0^2)^2\right], \quad (67)$$

where B_0, R_0, κ_0, q_0 are constant parameters. Using Eq. (67), the partial derivatives are written as

$$\frac{\partial\Psi}{\partial R} = \frac{B_0}{2R_0^2\kappa_0 q_0}[2RZ^2+\kappa_0^2(R^2-R_0^2)R], \frac{\partial\Psi}{\partial Z} = \frac{B_0}{R_0^2\kappa_0 q_0}R^2Z. \quad (68)$$

$$\frac{\partial^2\Psi}{\partial R^2} = \frac{B_0}{2R_0^2\kappa_0 q_0}[2Z^2+\kappa_0^2(3R^2-R_0^2)] \quad (69)$$

$$\frac{\partial^2\Psi}{\partial Z^2} = \frac{B_0}{R_0^2\kappa_0 q_0}R^2, \frac{\partial^2\Psi}{\partial R\partial Z} = \frac{2B_0}{R_0^2\kappa_0 q_0}RZ \quad (70)$$

$$(71)$$

The toroidal field function g is a constant function, $g = c_g R_0 B_0$, where c_g is a dimensionless constant.

1.5 Initial conditions

The initial conditions of the particle are given by specifying the initial location (R,ϕ,Z), initial parallel velocity $v_\parallel$, and the magnetic moment μ (which acts as a parameter since μ is exactly conserved). In some cases, we prefer to specify the initial velocity in terms of the initial kinetic energy ε and the initial pitch angle θ (the include angle between velocity and the local magnetic field). The relation between (ε,θ) and $(v_\parallel,\mu)$ is given by

$$\mu = \frac{mv_\perp^2}{2B} = \frac{mv^2}{2B}\sin^2\theta = \frac{\varepsilon}{B}\sin^2\theta, \quad (72)$$

and

$$v_\parallel = v\sin\theta = \sqrt{\frac{2\varepsilon}{m}}\cos\theta. \quad (73)$$

The relation between (ε,θ) and the normalized quantities $(\overline{\mu},\overline{v}_\parallel)$ is given by

$$\overline{\mu} = \frac{\mu}{\mu_n} = \frac{\varepsilon}{B}\sin^2\theta\frac{1}{mv_n^2/B_n} = \frac{\varepsilon}{mv_n^2\overline{B}}\sin^2\theta, \quad (74)$$

and

$$\overline{v}_\parallel = \sqrt{\frac{2\varepsilon}{mv_n^2}}\cos\theta. \quad (75)$$

——-

$$2(\varepsilon-B\mu)-\frac{1}{m}(P_\phi-Ze\Psi)^2\left(\frac{B}{g}\right)^2 = 0$$

$$2\left(1-\frac{B}{B_0}\lambda\right)-(P_\phi-Ze\Psi)^2\left(\frac{B}{g}\right)^2\frac{1}{m\varepsilon} = 0,$$

where $\lambda = B_0\mu/\varepsilon$

——

2 Benchmark of the code

There are three constants of motion for the guiding center motion, namely, the canonical toroidal angular momentum P_ϕ, the magnetic moment μ, and the total kinetic energey ε. Examining how well the kinetic energy ε

and the toroidal angular momentum P_ϕ are conserved provides a way to evaluate the accuracy of the numerical code. The kinetic energy ε and toroidal angular momentum P_ϕ are defined by

$$\varepsilon = \frac{1}{2} m v^2 = \frac{1}{2} m v_\parallel^2 + B\mu \tag{76}$$

$$P_\phi = m\frac{g(\Psi)}{B} v_\parallel + Ze\Psi, \tag{77}$$

Define $\varepsilon_n = m v_n^2$ and $P_{\phi n} = ZeB_n L_n^2$, then the normalized forms of ε and P_ϕ are written as

$$\bar{\varepsilon} \equiv \frac{\varepsilon}{m v_n^2} = \frac{1}{2}\bar{v}_\parallel^2 + \bar{\mu}\overline{B} \tag{78}$$

$$\begin{aligned} \overline{P}_\phi &\equiv \frac{P_\phi}{P_{\phi n}} \\ &= \frac{1}{2\pi}\bar{g}\frac{\overline{v}_\parallel}{\overline{B}} + \overline{\Psi} \end{aligned} \tag{79}$$

Figure 6 plots the time evolution of the kinetic energy $\bar{\varepsilon}$ and toroidal angular momentum $\overline{P}_\phi$ for an energetic ion in EAST magnetic configuration. The results shows that $\bar{\varepsilon}$ and $\overline{P}_\phi$ are conserved to acceptable accuracy for a long time (100 poloidal periods of the orbit).

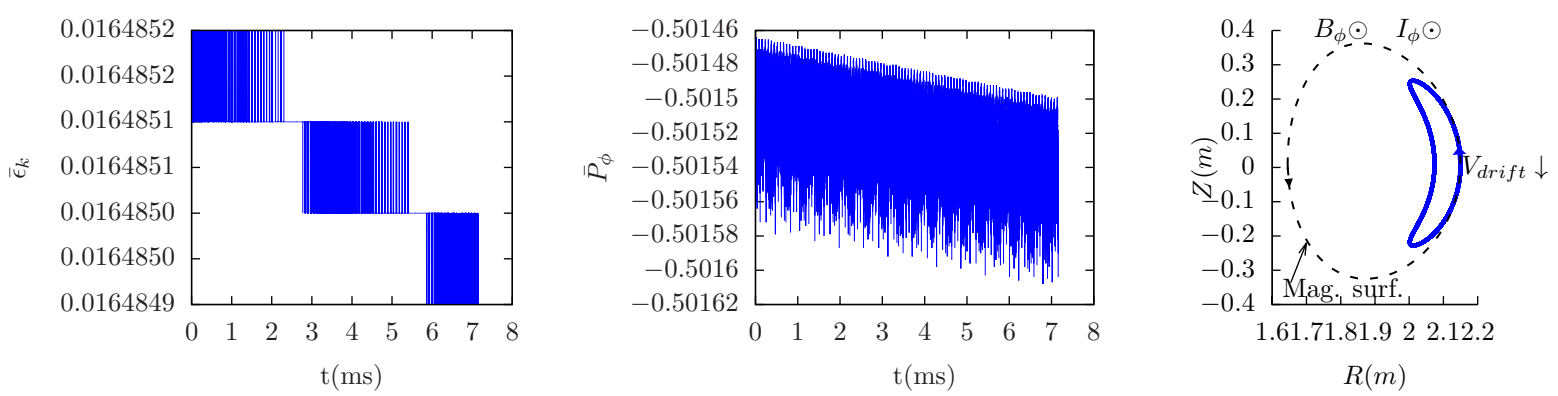

Figure 6. Time evolution of the kinetic energy $\bar{\varepsilon}$ (a) and toroidal angular momentum $\overline{P}_\phi$ (b) for a Deuteron of 20keV launched at the low-field-side midplane ($R_{\rm ini} = 2.15m, Z_{\rm ini} = 0m$) with pitch angle $\theta = 75°$. The results shows that $\bar{\varepsilon}$ and $\overline{P}_\phi$ are conserved to acceptable accuracy ($\bar{\varepsilon}_k$ decreased by 1.8×10^{-5} and $\bar{P}_\phi$ by 3.2×10^{-4} during the time of 100 poloidal periods). The corresponding poloidal orbit is plotted in (c). Fourth-order Runge-Kutta time advancing scheme is used in integrating the orbit with a time step of 1/183 poloidal period. The magnetic equilibrium is from EAST discharge #62585@2.8s (gfile provided by ZhengZheng).

2.1 Trapped and circulating particles

An approximate condition determining whether a particle is trapped or circulating can be obtained by using the conservation of magnetic moment and kinetic energy, and assuming the guiding center orbit is along the magnetic field line (zero-width orbit approximation, which is a proper approximation for low-energy particles whose orbit width is small, as is shown in Fig. 7).

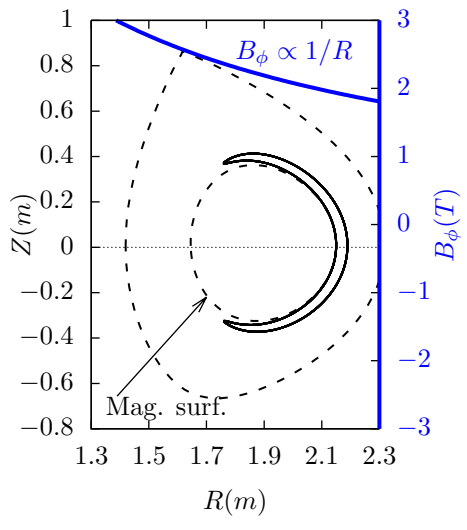

Figure 7. The magnetic field becomes stronger when a particle move inboard (toward smaller R). Due to the conservation of kinetic enery and magnetic moment, the magnitude of the paralell velocity decrease when a particle moves inboard. Also shown is the poloidal projection of guiding-center orbit for a particle of energy 2keV launched at the low-field-side midplane ($R = 2.25m, Z = 0m$) with a pitch angle $\theta = 115°$.

In this approximation, the orbit remains on a magnetic surface. The critical condition for a particle to be trapped or circulating is given by

$$\frac{m v_{I\perp}^2}{2B_I} = \frac{m v^2}{2B_{\max}}, \tag{80}$$

where $v_{I\perp}$ is the initial perpendicular (to the magnetic field) velocity of the particle, B_I is the strength of the magnetic field at the initial location of the particle, $B_{\max}$ is the maximum value of the magentic field on the same magnetic surface where the particle moves. Equation (80) can be written

$$\sin^2\theta_I = \frac{B_I}{B_{\max}}, \tag{81}$$

where $\theta_I = \arccos(v_{I\perp}/v)$ is the initial pitch angle of velocity with respect to the local magnetic field. It is obvious that particles with $\sin^2\theta_I > B_I/B_{\max}$ can not reach the point of the maximum magnetic field of the same magnetic surface and thus they are trapped particles. Otherwise, they are circulating particles. In velocity space $(v_\parallel, v_\perp)$, the trapped and circulating region are shown in Fig. 8.

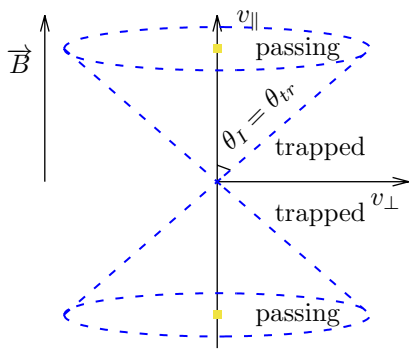

Figure 8. Passing and trapped regions in the phase-space $(v_\parallel, v_\perp)$. The boundary between passing and trapped region is given by $\theta_I = \theta_{\rm tr}$, where $\theta_{\rm tr}$ is determined by $\sin^2\theta_{\rm tr} = B_I/B_{\max}$; B_I and $B_{\max}$ are respectively the local (at the initial location of the particle) and maximal value of the magnetic field on one magnetic surface.

Note that the trapped-circulating boundary given in Fig. 8 is determined based on the assumption that the guiding center motion does not deviate from a magnetic surface. However, the actual guiding center orbit does not remain on the same magnetic surface, so the above result can be wrong when applied to some particles. An example is given in Fig. 9, where the numerical results show that the particle is actually trapped but the approximate condition indicate that the particle is circulating.

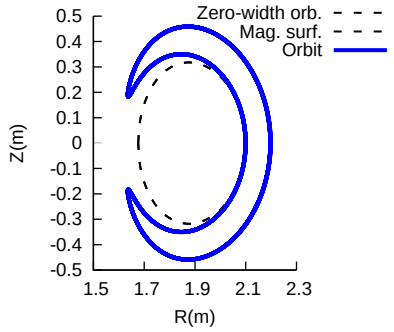

Figure 9. Numerical orbit of a particle on the poloidal plane, which show that the particle is trapped. However, the particle would be considered to be circulating if we used the approximate condition given in Fig. 8. It is easy to understand why the approximate condition breaks down for this case: the orbit derivates from the original flux surface (i.e., the zero-width orbit)to the stronger field region.

In terms of $(w,\ \mu)$ coordinates, where w is the kinetic energy, the trapped regions and the passing regions of pahse space are shown in Fig. 10.

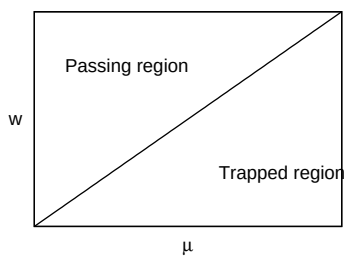

Figure 10. The passing and the trapped regions of phase space $(w,\ \mu)$. The boundary between passing and trapped region is given by $w = \mu B_{\max}$, where $B_{\max}$ is the maximum value of magnetic field on the same magnetic surface where the particle moves.

2.2 Analytical estimation of bounce frequency of deeply trapped particles

The time evolution of the paralell velocity of a guiding center is given by Eq. (2), i.e.,

$$\frac{dv_\parallel}{dt} = -\frac{\mu}{m}\frac{\mathbf{B}^\star}{B_\parallel^\star}\cdot\nabla B, \tag{82}$$

which can be approximately written as

$$\frac{dv_\parallel}{dt} = -\frac{\mu}{m}\mathbf{b}\cdot\nabla B,$$

which can be further written as

$$\frac{d^2l}{dt^2} = -\frac{v_\perp^2}{2B}\frac{dB}{dl} \tag{83}$$

where dl is the arc lengh along the magnetic field. In a large aspect ratio tokamak with circular flux surfaces, the magnetic field can be written approximatedly as

$$B = \frac{B_0}{1+(r/R_0)\cos\theta}, \tag{84}$$

The equation of magnetic field is written

$$\frac{B_\theta}{B} = \frac{dl_p}{dl} = \frac{r\,d\theta}{dl}, \tag{85}$$

which can be written

$$dl = \frac{B}{B_\theta} r\,d\theta \tag{86}$$

Using Eqs. (86) and (84), the paralel derivative of the magnetic field is written as

$$\frac{dB}{dl} = \frac{B_\theta}{rB}\frac{dB}{d\theta} = \frac{B_\theta}{rB}\frac{B_0}{[1+(r/R_0)\cos\theta]^2}\frac{r}{R_0}\sin\theta, \tag{87}$$

Using this, equation (83) is written

$$\frac{d^2l}{dt^2} = -\frac{v_\perp^2}{2B}\frac{B_\theta}{rB}\frac{B_0}{[1+(r/R_0)\cos\theta]^2}\frac{r}{R_0}\sin\theta = -\frac{v_\perp^2}{2}\frac{B_\theta}{B_0}\frac{1}{R_0}\sin\theta \tag{88}$$

Consider deeply trapped particles (particles are trapped in a very small region near the low-field-side midplane), i.e., $\theta \approx 0$, then we have $\sin\theta \approx \theta$. Using this, the above equation is written as

$$\frac{d^2l}{dt^2} \approx -\frac{v_\perp^2}{2}\frac{B_\theta}{B_0}\frac{1}{R_0}\theta \tag{89}$$

Assume the orbit is along the magnetic field line (i.e. zero-width orbit approximation), then the equation of magnetic field (86) is also satisfied by the orbit. In the linear approximation, we have $\theta \approx B_\theta/(Br)l$. Using this in Eq. (89), we obtain

$$\frac{d^2l}{dt^2} = -\frac{rv_\perp^2}{2R_0}\frac{B_\theta^2}{B^2r^2}l \tag{90}$$

Using the definition of safety factor, $q = rB_0/R_0B_\theta$, the above quation is written

$$\frac{d^2l}{dt^2} = -\frac{v_\perp^2}{q^2R_0^2}\frac{r}{2R_0}l \tag{91}$$

Define

$$\omega_b = \frac{v_\perp}{qR_0}\left(\frac{r}{2R_0}\right)^{1/2}, \tag{92}$$

(for deeply trapped particles, the variation of $v_\perp$ during one poloidal period is small, and thus can be considered constant, and thus ω_b can also be considered constant), then Eq. (91) is written

$$\frac{d^2l}{dt^2} = -\omega_b^2 l, \tag{93}$$

which indicates that the motion of a deeply trapped particle is a harmonic oscillation with an angular frequency ω_b. Equations (92) and (93) agree with Eqs. (3.12.3) and (3.12.4) in Wesson's book "Tokmaks"[2]. I have test the accuracy of formula (92) by comparing it with the numerical results, which indicates the formula can usually give a reasonable estimation of the bounce frequency (for example, 28kHz is obtained numerically while the analytical formula gives 24kHz for a not very deeply trapped orbit)

2.3 Methods of determining drift orbits

If neglecting the magnetic drift, a guiding-center orbit is along a magnetic field lines. Therefore there is no derivation from the magnetic surface where a guiding center is initially located. Taking the magnetic drift into account, a guiding-center orbit will deviate from the initial magnetic surface and the orbit will have finite-width.

Whether a drift orbit is inside or outside of the local magnetic surface near the midplane can be determined in the following way. First note that the zero-order approximation of the guiding-center orbit (zero-width orbit) is either parallel or anti-parallel to the local magnetic field, depending on the sign of $v_\parallel$. Further note the direction of the magnetic drift ($\mathbf{B} \times \nabla B$ and curvature drift) is approximatedly vertical, which can be either up or down, depending on the direction of the toroidal magnetic field. Finally, by imposing the magnetic drift on the zero-width orbit, we can determine whether the guiding center will drift inside or outside of the local magnetic surface. Figures 11-13 plots the drift orbits for all the possible combinitions of tokamak magnetic configurations and particle initial conditions.

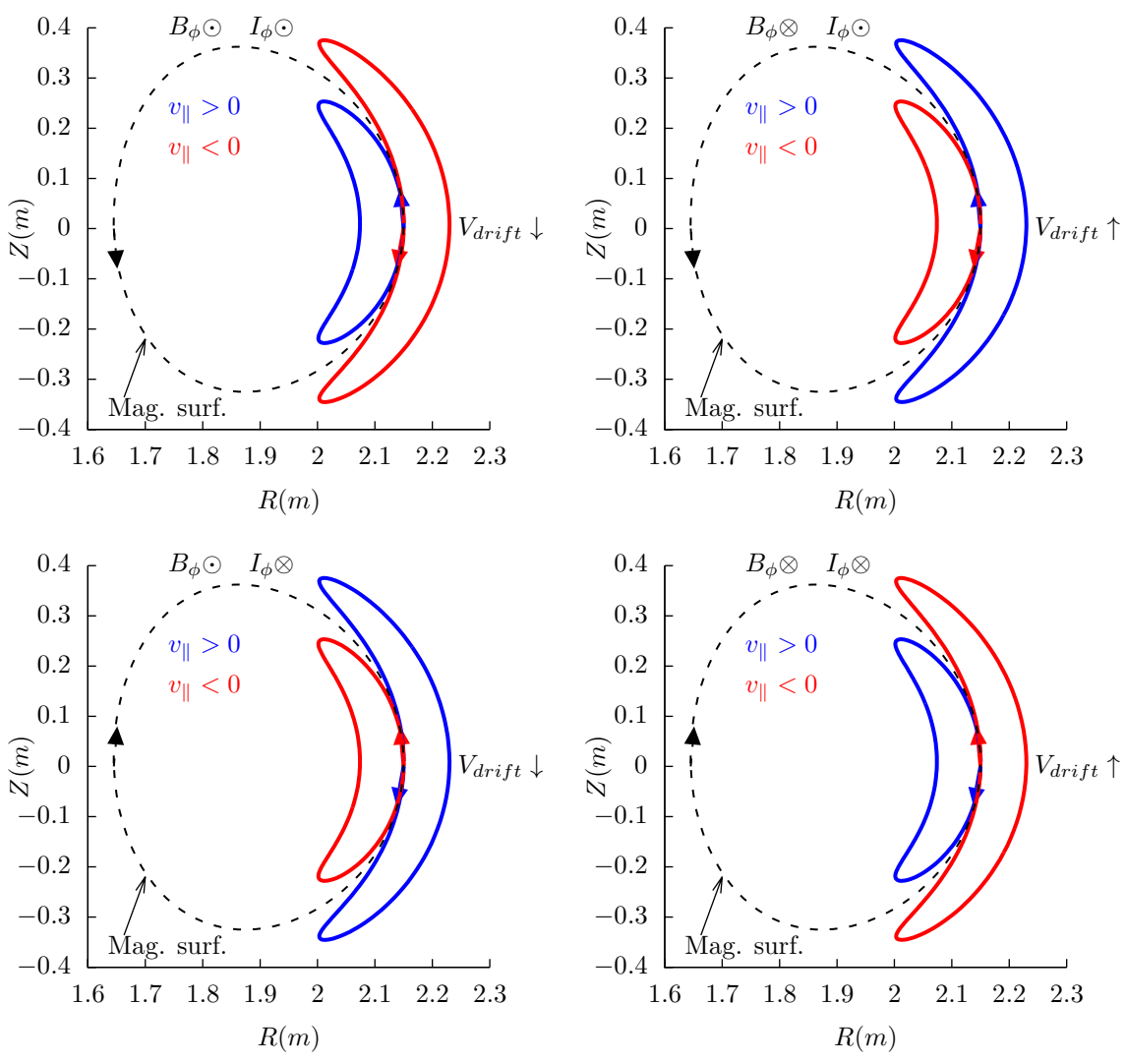

Figure 11. Projection of trapped orbits on the poloidal plane for various magnetic configurations. A Deuterium ion of 20keV is launched from the low-field-side midplane ($R_{\text{initial}} = 2.15m$, $Z_{\text{initial}} = 0m$) with pitch angle $\theta = 75°(v_\parallel > 0)$ and $\theta = 105°(v_\parallel < 0)$. $v_\parallel > 0$ implies that the zero-width orbit in the poloidal plane is along the direction of the poloidal magnetic field, which is in turn determined by the direction of the toroidal plasma current. The magnetic equilibrium is from EAST discharge #62585@2.8s (gfile provided by ZhengZheng). The direction of toroidal plasma current, magnetic field, and the corresponding magnetic drift are indicated on the figures.

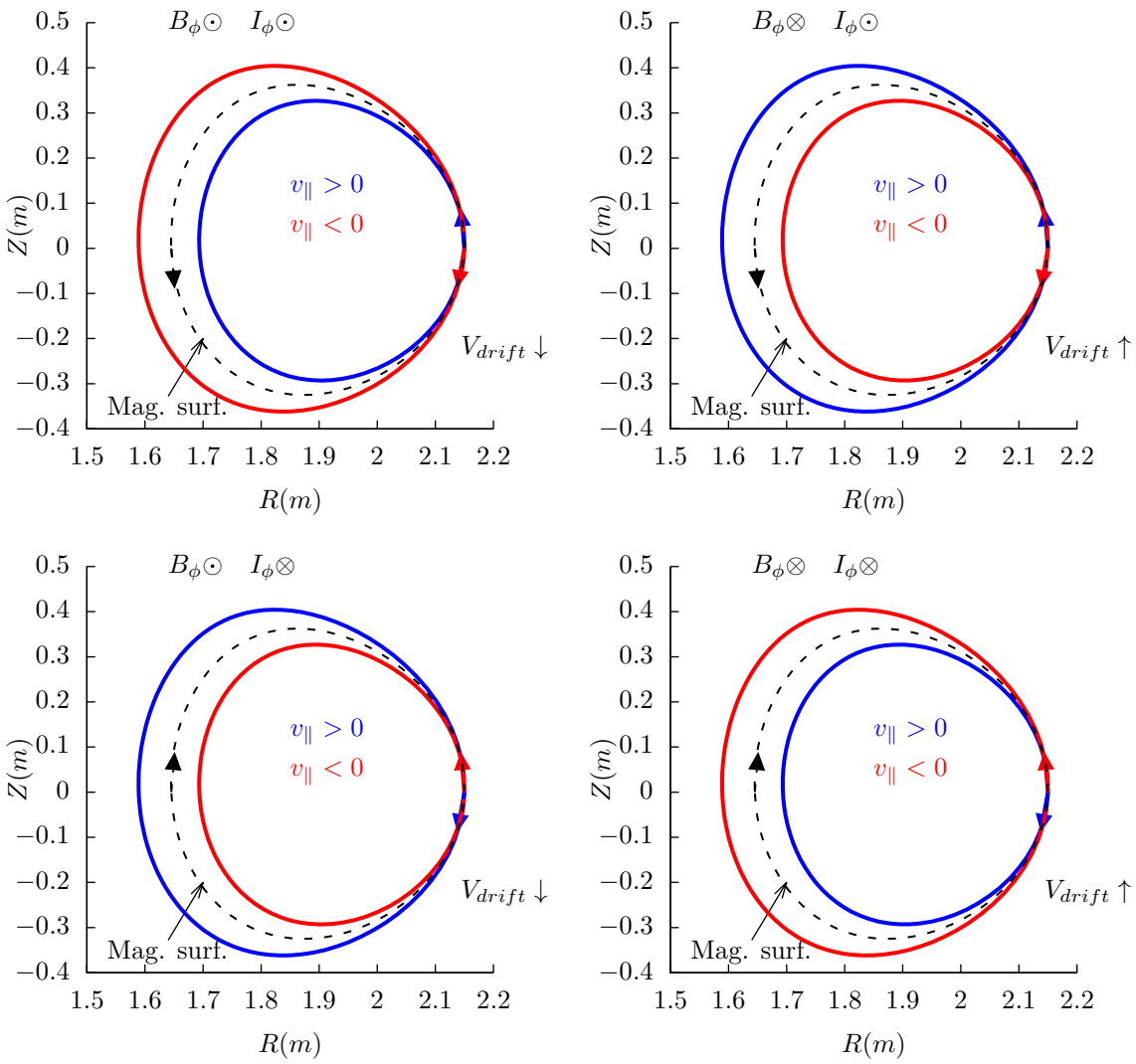

Figure 12. Projection of passing orbits on the poloidal plane for various magnetic configurations. A Deuterium ion of 20keV is launched from the low-field-side midplane ($R_{\rm ini} = 2.15m$, $Z_{\rm ini} = 0m$) with pitch angle $\theta = 50°(v_\parallel > 0)$ and $\theta = 130°(v_\parallel < 0)$. The magnetic equilibrium is from EAST discharge #62585@2.8s (gfile provided by ZhengZheng). The direction of plasma current, magnetic field, and the corresponding magnetic drift are indicated on the figures.

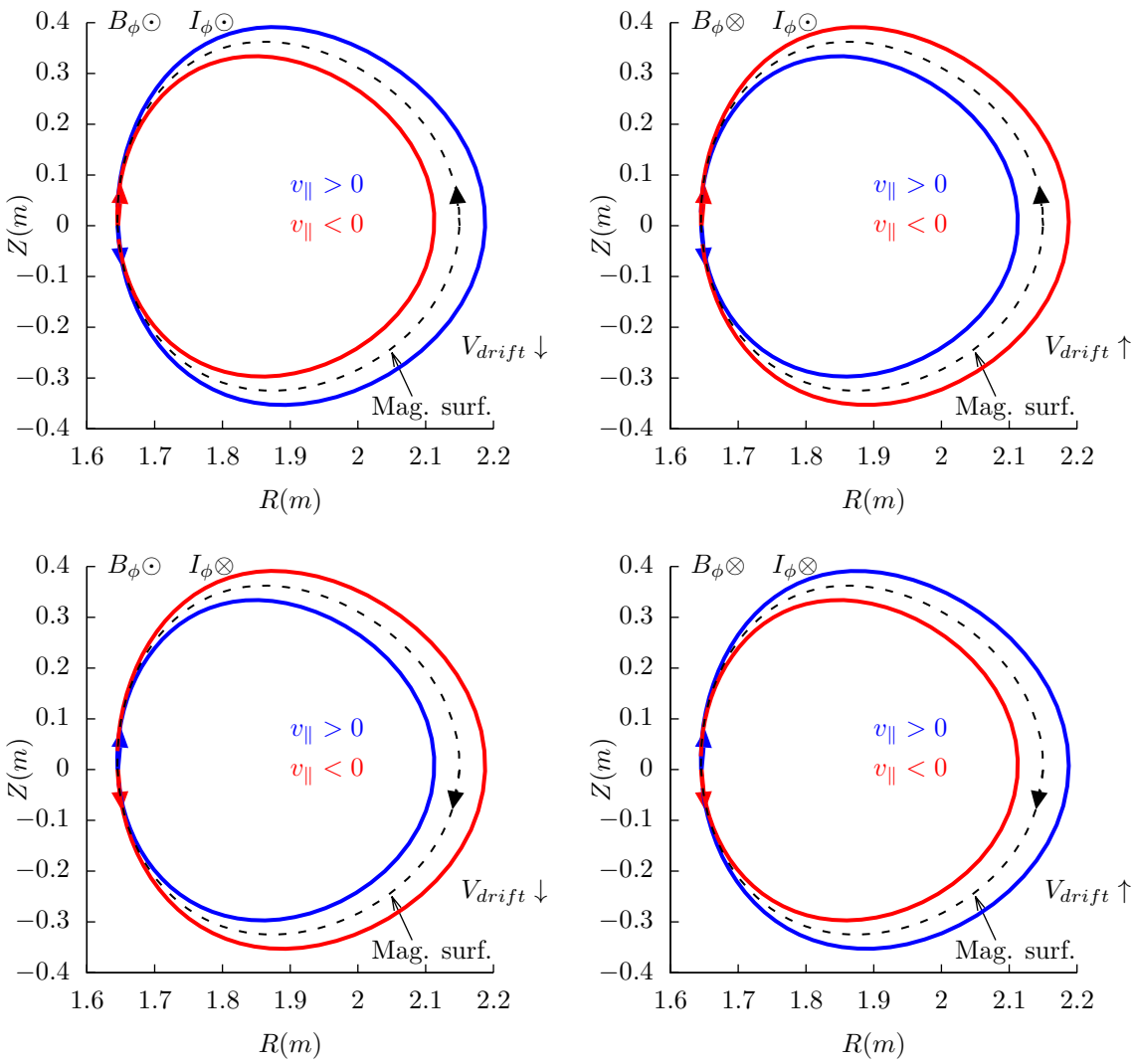

Figure 13. Projection of passing orbits on the poloidal plane for various magnetic configurations. A Deuterium ion of 20keV is launched from the high-field-side midplane ($R_{\rm ini} = 1.6452m$, $Z_{\rm ini} = 0m$) with pitch angle $\theta = 50°(v_\parallel > 0)$ and $\theta = 130°(v_\parallel < 0)$. The magnetic equilibrium is from EAST discharge #62585@2.8s (gfile provided by ZhengZheng). The direction of plasma current, magnetic field, and the corresponding magnetic drift are indicated on the figures.

Examining the above results, it is ready to realize that reversing the direction of the toroidal magnetic field does not change the projection of orbits on the poloidal plane, i.e., the location and shape of the poloidal orbits remain the same. However the direction of the poloidal motion is changed from clockwise (anti-clockwise) to anti-clockwise (clockwise). (This is obvious because $v_\parallel$ of a particle changes sign when the toroidal field is reversed and thus the direction of the poloidal motion changes).

Examining the above results, we can also find that, for particles launched from low-field-side midplane, co-current partilces have their orbits inside the magnetic surface at which the particle is iniitally located, and counter-current particles have thier orbits outside of the magnetic surface. For particles launched from the high-field-side midplane, the conclusion is reversed, i.e., co-current partilces have their orbits outside the magnetic surface where they are iniitally located, and counter-current particles have thier orbits inside of the magnetic surface.

These conclusions have important implications for the neutral beam injection, where orbits outside a reference

magnetic surface are more likely to be lost to the wall of the machine. If the neutral beam injection (NBI) is along the same direction of the plasma current, it is called the co-current injection. Otherwise it is called the counter-current injection. Using the above conclusions, we know that, for co-current injection, ions ionized at the low-field-side have better confinement compared with those ionized at the high-field-side. For the counter-current injection, ions ionized at the high-field-side have better confinement compared with those ionized at the low-field-side. Whether the overall confinment of ions due to co-current injection is better or worse than that of the counter-current injection depends on the ratio of number of ions deposited at the low-field-side to that deposited at the high-field side. For the shine-through loss to be small, most neutral must ionize at the low-field-side (most neutrals ionizing at the the high-field side usually means a very high shine-through loss fraction (>50%)). Therefore, under the assumption that most neutral beam particles are ionized on the low-field-side, it is right to say that co-curent injection is better than counter-current injection.

Figure 14 and 15 compares the poloidal orbits of energetic Deuterium particles ionized at the low-field-side midplane due to co-current and counter-current injection. The results indicate again that the counter-injected particles ionized at the low-field-side midplane are easy to be lost from the plasma because their orbits are outside the flux surface where they are ionized, and thus are more likely to touch the first wall.

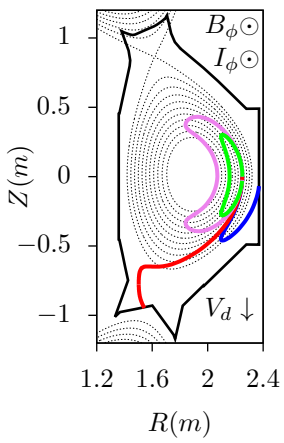

Figure 14. Poloidal orbits of Deuterium particles of 50keV ionized at the low-field-side midplane ($R = 2.25m$, $Z = 0m$) with a birth pitch angle $\theta = 125°$ (red), $\theta = 105°$ (blue), $\theta = 75°$ (green), and $\theta = 65°$ (violet). Pitch angle θ is the included angle between the magnetic field and the velocity of particles. Since the magnetic field and the plasma current are in the same direction for this case, $\theta > 90°$ means counter-current injection and $\theta < 90°$ means co-current injection. The counter-injected particles are easy to be lost from the plasma because their orbits are outside the flux surface where they are ionized, and thus are more likely to touch the first wall. The magnetic equilibrium is for EAST discharge #62585@2.8s, which is a upper single-null configuration (gfile provided by ZhengZheng).

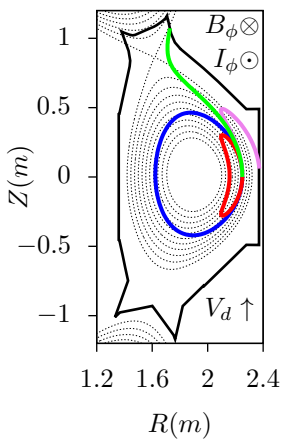

Figure 15. Poloidal orbits of Deuterium particles of 50keV ionized at the low-field-side midplane ($R = 2.25m$, $Z = 0m$) with a birth pitch angle $\theta = 125°$ (blue), $\theta = 105°$ (red), $\theta = 75°$ (violet), and $\theta = 60°$ (green). Since the magnetic field and the plasma current are in the opposite direction for this case, $\theta > 90°$ means co-current injection and $\theta < 90°$ means counter-current injection. The magnetic equilibrium is from EAST discharge #62585@2.8s but with the direction of the toroidal magnetic field reversed.

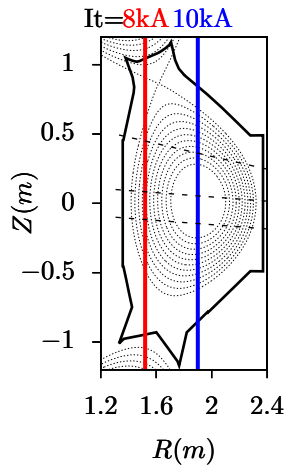

Figure 16. The resonant layer of 50MHz electromagnetic wave with the third harmonic of ion cyclotron frequency on EAST tokamak. The toroidal magnetic field of EAST is approximately given by $B_\phi = 4.160 \times 10^{-4} I_s / R$, where I_s is the current in a single turn of the TF coils, which in in the range from $8000A$ to $10000A$ for usual EAST discharges. The ion cyclotron angular frequency is given by $\omega_{ci} = B_\varphi e / m_i$ ($f_{ci} = \omega_{\rm ci} / 2\pi$). The small Dopper frequency shift $k_\parallel v_\parallel$ is not included in the estimation of the resonant layer.

2.4 Toroidal procession

Figure 17 plots the guiding centers orbits for particles launched at the low-field-side of the midplane with different values of the pitch angle θ.

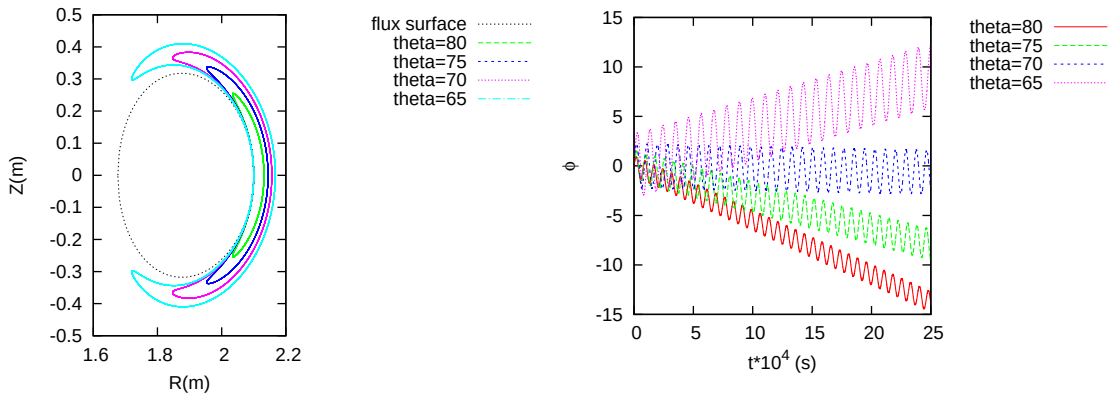

Figure 17. Left: projection of guiding center orbits of trapped particles on (R, Z) plane. Right: Toroidal motion of guiding center of the trapped particles. All particles have the same kinetic energy $\varepsilon = 10$keV and are launched from the low-field side midplane of the reference magnetic surface ($R = 2.1$, $Z = 0$). The equilibrium is a Solovev equilibrium with $R_0 = 1.9m$, $B_0 = 2.0$Tesla, $\kappa_0 = 1.5$, $Ze_0 = 1.5$, $g = 3.8$mT.

Figure 17 shows (1) the toroidal procesion of deeply trapped particles is faster than that of the shallowly trapped particles and (2) the direction of the toroidal precession of the particle with $\theta = 65°$ is different from the others.

Procession angular frequency of a trapped particles (from Porcelli's slide):

$$\omega_D = \frac{v^2}{2\Omega_c R r} = \frac{E_k}{BZeRr}, \tag{94}$$

where E_k is the kinetic energy of the particle. Equation () indicates that the procession frequency is proportional to the energy of the particle.

$$\omega_D = \frac{v^2}{2\Omega_c R r} = \frac{v^2}{2\overline{B}\Omega_n \overline{R}\,\overline{r} L_n^2} = \Omega_n \frac{\overline{v}^2}{8\pi^2 \overline{B}\,\overline{R}\,\overline{r}} \tag{95}$$

Compared with the results given by the numerical code, the above results seems to be roughly correct when the orbit is not near the magnetic axis.

$$\overline{v}_\perp^2 = \frac{v_\perp^2}{v_n^2} = \frac{2B\mu}{m v_n^2} = \overline{B}\frac{2B_n \mu}{m v_n^2} = 2\overline{B}\overline{\mu} \tag{96}$$

2.5 Radial drift –check!!

$$\frac{d\Psi}{dt} = \mathbf{V}_d \cdot \nabla\Psi = \frac{1}{\Omega}\mathbf{b} \times \left(\frac{\mu}{m}\nabla B + v_\parallel^2 \boldsymbol{\kappa}\right) \cdot \nabla\Psi$$

$$\frac{d\Psi}{dt} = \frac{1}{B\Omega}\mathbf{B} \times \left(\frac{\mu}{m}\nabla B + v_\parallel^2 \boldsymbol{\kappa}\right) \cdot \nabla\Psi$$

$$\frac{d\Psi}{dt} = -\frac{1}{B\Omega}\mathbf{B} \times \nabla\Psi \cdot \left(\frac{\mu}{m}\nabla B + v_\parallel^2 \boldsymbol{\kappa}\right)$$

using

$$\mathbf{B} = \nabla\Psi \times \nabla\phi + g\nabla\phi$$

$$\frac{d\Psi}{dt} = -\frac{1}{B\Omega}(\nabla\Psi \times \nabla\phi \times \nabla\Psi + g\nabla\phi \times \nabla\Psi) \cdot \left(\frac{\mu}{m}\nabla B + v_\parallel^2 \boldsymbol{\kappa}\right) \tag{97}$$

Noting that both ∇B and $\boldsymbol{\kappa}$ are approximatedly along $-\hat{\mathbf{R}}$ direction, which is perpendicular to $\nabla\phi$, Eq. (97) is written as

$$\frac{d\Psi}{dt} = -\frac{1}{B\Omega}(g\nabla\phi \times \nabla\Psi) \cdot \left(\frac{\mu}{m}\nabla B + v_\parallel^2 \boldsymbol{\kappa}\right)$$

$$\frac{d\Psi}{dt} = \frac{1}{B\Omega} g\mathbf{B}_p \cdot \left(\frac{\mu}{m}\nabla B + v_\parallel^2 \boldsymbol{\kappa}\right)$$

if

$$\frac{d\Psi}{dt}(\Psi_{\text{lcfs}} - \Psi_{\text{axis}}) > 0,$$

then the drift from the local magnetic surface is outward, otherwise, the drift is inward.

$$\frac{d\Psi}{dt}(\Psi_{\text{lcfs}} - \Psi_{\text{axis}}) = \frac{1}{B\Omega} g\mathbf{B}_p \cdot (-\hat{\mathbf{R}})(\Psi_{\text{lcfs}} - \Psi_{\text{axis}})$$

Examining the right-hand side of Eq. (97), we find that $\mathbf{B}_p$ and $(\Psi_{\text{lcfs}} - \Psi_{\text{axis}})$ change signs simutaneouslly when the toroidal plasma current I_ϕ change sign, thus the direction of $\mathbf{B}_p(\Psi_{\text{lcfs}} - \Psi_{\text{axis}})$ is independent of the sign of I_ϕ. Therefore the sign of the radial drift is independent of the sign of I_ϕ.

2.6 Width of guiding center orbit

The gyroradius of a particle is given by $r = mv/BZe$, which can be further written as

$$r = \frac{\sqrt{2m\varepsilon}}{BZe}, \tag{98}$$

where ε is the kinetic energy of the particle. For an electron with the same kinetic energy of a ion, Eq. (98) indicates that the gyroradius of the electron is smaller than that of the ion by the factor $\sqrt{m_e/m_i}$. Now comes the question: Is the width of the guiding center orbit of an electron with the same kinetic energy of a ion smaller than that of the ion? Examine one of the constant of motion, P_ϕ, which is given by

$$\frac{P_\phi}{Ze} = \frac{g(\Psi)}{\Omega} v_\parallel + \Psi, \tag{99}$$

The function $g(\Psi)/\Omega$ is usually a weak function of Ψ, thus can be asssumed to be a contant. The orbit width can be characterised by $\Delta\Psi$, which is written

$$\Delta\Psi = -g\frac{\Delta v_\parallel}{\Omega} = -g\frac{m\Delta v_\parallel}{BZe}, \tag{100}$$

where $\Delta v_\parallel$ is the variation range of $v_\parallel$ in one poloidal period of the orbit. For trapped particles, this variation can be approximated as

$$\Delta v_\parallel \approx v_t = \sqrt{\frac{2T}{m}} \tag{101}$$

Using this, Eq. (100) is written as

$$\Delta\Psi = -g\frac{\sqrt{m}\sqrt{2T}}{BZe}, \tag{102}$$

which indecates that, for the same temperature, $\Delta\Psi$ is proportional to $\sqrt{m}$. (For circulationg ions, the variation of $v_\parallel$ during one poloidal period can not be approximated by v_t. Thus I do not know how to estimate the orbit width).

The variation of the poloidal flux $\Delta\Psi$ can be approximated by

$$\Delta\Psi = 2\pi R\Delta r B_p \tag{103}$$

where Δr is the variation of the minor radius, B_p is the poloidal magnetic field. Using this in Eq. (102), we obtain

$$\Delta r = -g\frac{\sqrt{2mT}}{2\pi R B_p BZe} \approx -\frac{\sqrt{2mT}}{2\pi B_p Ze}, \tag{104}$$

which indicates that the width of guiding-center orbits is inversely proportional to the poloidal magnetic field B_p, instead of the toroidal magnetic field B_t (first got to know this conclusion from J. Wession's book "Science of JET", and later wrote the above derivation). This explains why high plasma current is beneficial to the confinement of energetic particles (because high current corresponds to higher poloidal magnetic field B_p and smaller orbit width and thus better confinement of energetic particles which usually have larger orbit width than thermal particles).

A numerical example in Fig. 18 indicate, as expected, that the guiding center orbit width of an electron with the same kinetic energy of a ion is much smaller than that of the ion.

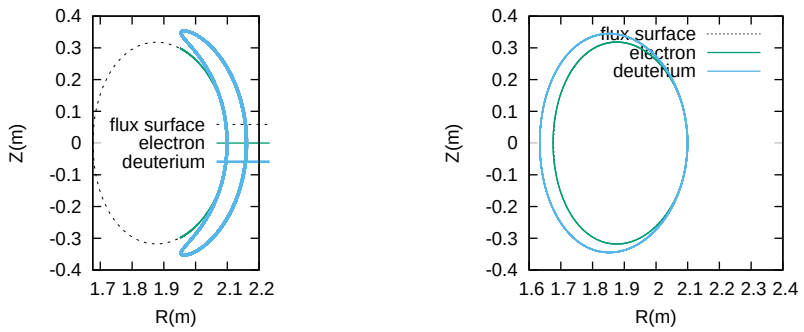

Figure 18. Comparision of the guiding center orbit width of an electron and a Deuteron that have the same value of kinetic energy (20keV). Particles are launched from the low field side of the midplane of the reference flux surface ($R = 2.1m, Z = 0.0m$) with pitch angle $\theta = 75°$ (left graph) and $\theta = 55°$ (right graph). The results show that the orbit width of electron is negligibly small (compared with that of the Deuteron) and the orbit almost coincides with the magnetic surface.

2.7 3D trajectory of guiding-center

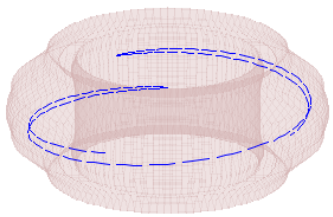

Figure 19. Three-dimensional illustration of the guidieng-center orbit of a trapped particle in a tokamak.

2.8 Trapped particle fraction

The trapped particle fraction f_t is defined as the ratio of the number of trapped particles to the total number of particles. Using spherical coordinates in velocity space, the particle distribution function can be written as $f = f(\mathbf{r}, v, \theta, \phi)$, where $\mathbf{r}$ is the location vector in configuration space, (v, θ, ϕ) is the spherical coordinates in velocity space with θ being the pitch angle. Then the trapped particle fraction f_t is written as

$$f_t(\mathbf{r}) = 1 - \frac{2\int_0^\infty \int_0^{\theta_{\rm tr}} f(v,\theta,\varphi) v^2 \sin\theta dv d\theta d\phi}{\int_0^\infty \int_0^{\pi} f(v,\theta,\varphi) v^2 \sin\theta dv d\theta d\phi}, \tag{105}$$

where $\theta_{\rm tr}$ is the critical pitch angle defined in Sec. 2.1; the numerator of the fraction in Eq. (105) is the number of passing particles. Assuming f is independent of ϕ, then the above equation is written as

$$f_t(\mathbf{r}) = 1 - \frac{2\int_0^\infty \int_0^{\theta_{\rm tr}} f(v,\theta) 2\pi v^2 \sin\theta dv d\theta}{\int_0^\infty \int_0^{\pi} f(v,\theta) 2\pi v^2 \sin\theta dv d\theta}. \tag{106}$$

If we further assume f is independent of θ, i.e., f is isotropic in velocity space, then Eq. (106) is written

$$\begin{aligned} f_t &= 1 - \frac{4\pi(1-\cos\theta_{\rm tr})\int_0^\infty f v^2 dv}{4\pi\int_0^\infty f v^2 dv} \\ &= \cos\theta_{\rm tr} \end{aligned} \tag{107}$$

The critical angle $\theta_{\rm tr}$ in the zero-orbit-width approximation is given by

$$\sin^2\theta_{\rm tr} = \frac{B_I}{B_{\rm max}}. \tag{108}$$

Using this in Eq. (107) yields

$$f_t = \sqrt{1-\frac{B_I}{B_{\rm max}}} \tag{109}$$

In the large aspect ratio approximation and for particles that are initially at the low-field-side of the midplane, Eq. (109) is written

$$f_t = \sqrt{1-\frac{R_0-r}{R_0+r}} = \sqrt{\frac{2r}{R_0+r}}. \tag{110}$$

This is the result given in Wessson's book[2]. Note that this result is valid only for particles that are initially at the low-field-side of the midplane. For particles that are initially located at the poloidal location θ_p, the trapped particles fraction is written

$$f_t = \sqrt{1-\frac{R_0-r}{R_0+r\cos\theta_p}} = \sqrt{\frac{r(1+\cos\theta_p)}{R_0+r\cos\theta_p}}, \tag{111}$$

For $\theta_p=\pi$, i.e., at the high-field-side of the midplane, $f_t=0$, i.e., there is no trapped particles there.

Using Eq. (111), the flux surface averaging of f_t, $\langle f_t\rangle$, is written as

$$\begin{aligned}\langle f_t\rangle &= \frac{\oint f_t \frac{1}{B_p} dl_p}{\oint \frac{1}{B_p} dl_p} \\ &= \frac{\oint \sqrt{\frac{r(1+\cos\theta_p)}{R_0+r\cos\theta_p}}\,\frac{1}{B_p} dl_p}{\oint \frac{1}{B_p} dl_p} \\ &= \frac{\oint \sqrt{\frac{r(1+\cos\theta_p)}{R_0+r\cos\theta_p}}\,\frac{1}{B_p} r\,d\theta}{\oint \frac{1}{B_p} r\,d\theta}\end{aligned}$$

3 Numerical results of prompt loss of fast ions

The initial distribtuion function of fast ions are assumed to take the following form:

$$f(\psi,v,\lambda) = C\exp\left(-\frac{\psi}{\psi_{\rm scale}}\right)\frac{1}{v^3+v_{\rm crit}^3}\frac{1}{2}{\rm erfc}\left(\frac{v-v_{\rm birth}}{\Delta_v}\right)\exp\left(-\frac{(\lambda-\lambda_0)^2}{\Delta_\lambda^2}\right), \tag{112}$$

where the constant C is set to achieve desired stored energy of energetic particles. Figure 20 plots the time evolution of the loss fraction due to the prompt loss (also called first orbit loss) in EAST#48916 at 4.6s.

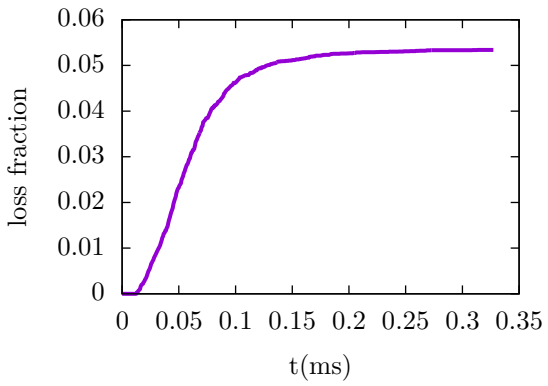

Figure 20. Time evolution of fast ions loss fraction in EAST discharge #48916 at 4.6s. Fast ions distribution function is given by Eq. (112).

$$d\Gamma = dV_s dV_v = R\,d\,R\,d\,Z\,d\phi 2\pi\frac{B}{m}\,dv_\parallel' d\mu$$

$$\frac{d\Gamma}{L_n^3 v_n^3} = \overline{R}\,d\,\overline{R}\,d\,\overline{Z}\,d\phi 2\pi\frac{B}{m v_n^2}\,d\overline{v}_\parallel' d\mu = \overline{R}\,d\,\overline{R}\,d\,\overline{Z}\,d\phi 2\pi\frac{\overline{B}}{m v_n^2/B_n}\,d\overline{v}_\parallel' d\mu = \overline{R}\,d\overline{R}\,d\overline{Z}\,d\phi 2\pi\overline{B}\,d\overline{v}_\parallel' d\overline{\mu} \tag{113}$$

Marker's phase-space volume V_j

4 Use constants of motion to determine orbit loss

This section discusses determining the prompt loss of ions by using the constants of motion. This work was motivated by Dr. Chengkang Pan, who shares an office with me and recently (2014) published a NF paper discussing this topic.

4.1 Critical velocity for ions loss

There are three constants of motion for the guiding center orbit, namely, the canonical toroidal angular momentum P_ϕ, the magnetic moment μ, and the total kinetic energey ε, which are given, respectively, by

$$P_\phi = m\frac{g(\Psi)}{B}\, v\xi + Ze\Psi, \tag{114}$$

$$\mu = \frac{m}{B} v^2(1-\xi^2), \tag{115}$$

$$\varepsilon = \frac{1}{2} m\, v^2, \tag{116}$$

where $g(\Psi) = RB_\phi$, ξ is the cosine of the pitch angle of guiding center velocity (with respect to the local magnetic field), $\Psi = RA_\phi$ with A_ϕ being the toroidal component of the magnetic vector potential, Ze ($e>0$) and m are the charge and mass of the ion, respectively.

Next, we use the constraint of the three constants of motion to determine whether an ion with a given initial condition can reach a boundary magnetic surface labeled by Ψ_a. The initial conditions of an ion is denoted with (Ψ_0, B_0, v_0, ξ_0), where Ψ_0 lables the flux surface where the particle is initially located, B_0 is the magnetic field strength at the initial location of the guiding-center, v_0 and ξ_0 are the initial velocity and pitch angle. The conditions of the particle when it reach the boundary flux surface are denoted with (Ψ_a, B_a, v_a, ξ_a). Then the conservation of P_ϕ requires

$$m\,\frac{g(\Psi_0)}{B_0}\, v_0\xi_0 + e\Psi_0 = m\,\frac{g(\Psi_a)}{B_a}\, v_a\xi_a + e\Psi_a. \tag{117}$$

Using the conservation of the kinetic energy, the above equation is written

$$m\, v_0\left(\frac{g(\Psi_0)}{B_0}\xi_0 - \frac{g(\Psi_a)}{B_a}\xi_a\right) = e(\Psi_a - \Psi_0). \tag{118}$$

Using the conservation of μ, we obtain

$$\frac{1-\xi_a^2}{B_a} = \frac{1-\xi_0^2}{B_0}, \tag{119}$$

which can be written

$$\xi_a = \pm\sqrt{1-\frac{B_a}{B_0}(1-\xi_0^2)}, \tag{120}$$

Using Eq. (120), equation (118) is written

$$m\, v_0\left[\frac{g(\Psi_0)}{B_0}\xi_0 \mp \frac{g(\Psi_a)}{B_a}\sqrt{1-\frac{B_a}{B_0}(1-\xi_0^2)}\right] = e(\Psi_a - \Psi_0), \tag{121}$$

which can be arranged in the form

$$v_0 = \frac{e(\Psi_a-\Psi_0)}{m}\left(\frac{g(\Psi_0)}{B_0}\xi_0 \mp \frac{g(\Psi_a)}{B_a}\sqrt{1-\frac{B_a}{B_0}(1-\xi_0^2)}\right)^{-1}, \tag{122}$$

Equation (122) gives the velocity v_0 needed for the particle to reach the flux surface Ψ_a. The value of v_0 given by Eq. (122) varies, depending on the value of B_a, i.e., depending on the poloidal location on the boundary magnetic flux surface. By varying the poloidal location on the boundary flux surface, we can obtain the minimum value of v_0, $v_{0\,\min}$, which is the minumu velocity for a particle with the initial condition (Ψ_0, B_0, ξ_0) to reach flux surface Ψ_a.

The above derivation does not distinguish between circulating particles and trapped particles. Next, we distinguish between these two kinds of particles. If the ion is a circulating one, then $v_\parallel$ does not change sign and thus ξ does not change sign either. In this case, equation (120) is written

$$\xi_a = \mathrm{sign}(\xi_0)\sqrt{1-\frac{B_a}{B_0}(1-\xi_0^2)}. \tag{123}$$

If the ion is a trapped one, then both signs $\pm$ in Eq. (120) are possible.

To evaluate the minimum energy for the ions to be lost, we need choose a equilibrium. Next, we give a simple large aspect ratio equilibrium.

4.2 Large aspect ratio equilibrium

Define (r,θ) coordinates by

$$R(r,\theta)=\overline{R}+r\cos\theta, \tag{124}$$

$$Z(r,\theta)=r\sin\theta, \tag{125}$$

The leading order equation of the Grad-Shafranov equation in $(r,\,\theta)$ coordinates is written (refer to my notes on tokamak equilibrium)

$$\frac{1}{r}\frac{d}{dr}r\frac{d\Psi}{dr}=-\mu_0\overline{R}J_\phi(r), \tag{126}$$

which gives concentric circular flux surfaces centered at $(R=\overline{R},Z=0)$. Assume that J_ϕ is uniform distributed, i.e., $|J_\phi|=I/(\pi a^2)$, where I is the total current within the flux surface $r=a$. Further assume the current is in the opposite direction of $\nabla\phi$, then $J_\phi=-I/(\pi a^2)$. Using this, Eq. (126) can be solved to give

$$\Psi=\frac{\mu_0 I}{4\pi a^2}\overline{R}r^2. \tag{127}$$

In (r,θ) corrdintates, the gradient of Ψ is written

$$\nabla\Psi=\frac{\mu_0 I}{2\pi a^2}\overline{R}r\hat{\mathbf{e}}_r \tag{128}$$

$$\begin{aligned}\mathbf{B}_p &= \nabla\Psi\times\nabla\phi\\ &= \frac{\mu_0 I}{2\pi a^2}\overline{R}r\hat{\mathbf{e}}_r\times\hat{\mathbf{e}}_\phi\frac{1}{R}\\ &= \frac{\mu_0 I}{2\pi a^2}\overline{R}\frac{r}{R}\hat{\mathbf{e}}_\theta\\ &= \frac{\mu_0 I}{2\pi a^2}\frac{r}{1+\frac{r}{\overline{R}}\cos\theta}\hat{\mathbf{e}}_\theta\end{aligned} \tag{129}$$

where $\hat{\mathbf{e}}_\theta$ is the unit vector along the direction of increassing θ (count-clockwise when looking along $\nabla\phi$). Define $\rho=r/a$ and $\varepsilon=a/\overline{R}$, then Eq. (129) is written

$$\mathbf{B}_p=\frac{\mu_0 I}{2\pi a}\frac{\rho}{1+\rho\varepsilon\cos\theta}\hat{\mathbf{e}}_\theta.$$

The toroidal component of the magnetic field is written

$$B_\phi=\frac{g(\Psi)}{R}=\frac{g(\Psi)}{\overline{R}+r\cos\theta}. \tag{130}$$

Consider the case that $g(\Psi)$ is a contant function, $g(\Psi)=B_{\phi 0}\overline{R}$, then Eq. (130) is written

$$B_\phi=\frac{B_{\phi 0}}{1+\frac{r}{\overline{R}}\cos\theta}=\frac{B_{\phi 0}}{1+\rho\varepsilon\cos\theta}. \tag{131}$$

$$B=\sqrt{B_\phi^2+B_\theta^2}=\sqrt{\left(\frac{\mu_0 I}{2\pi a}\rho\right)^2+B_{\phi 0}^2}\frac{1}{1+\rho\varepsilon\cos\theta}. \tag{132}$$

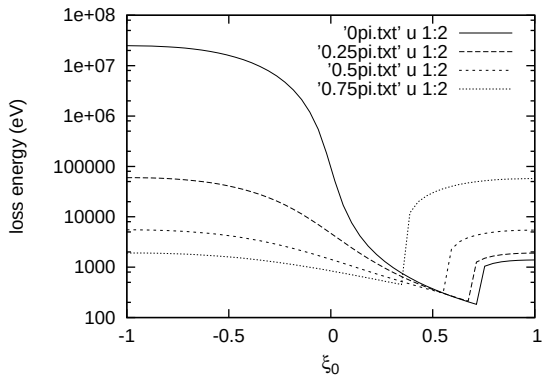

Figure 21. Minimus loss energy as a function of the cosine of the launching pitch angle. $\rho=0.98$

The minimum value of v_0, denoted with $v_{0\,\min}$, is reached when $\theta=\pi$ or $\theta=0$ depends on the $\pm$ in Eq. (160).

$$v_0 = \frac{e}{mR_0}\frac{\mu_0 I}{4\pi a^2}\overline{R}(a^2-r^2)\left(\xi_0 \mp \mathrm{sign}(\xi_0)\frac{\overline{R}+a}{\overline{R}+r}\sqrt{1-\frac{\overline{R}+r}{\overline{R}+a}(1-\xi_0^2)}\right)^{-1}. \tag{133}$$

$$v_{0\,\min}(\xi_0) = \max\left(\min\left(v_0(\xi_0,\theta)\right),0\right) \tag{134}$$

(in practice ψ_a is usually different from the actual poloidal flux Ψ_p and is related to Ψ_p by $\psi_a = \pm|\Psi_p|/2\pi + C$, where C is a constant)

Circulating region

$$1-\xi^2 < \frac{B_{\min}}{B_{\max}} \tag{135}$$

we consider the confinement of the particles. The method is to determine whether the particles can reach a boundary flux surface by making use of the three constants of the motion. The boundary flux surface is labled by ψ_a, where ψ_a is the poloidal flux within that flux surface.

Next examine what the conservation of P_ϕ, μ, and ε requires if the particle can reach the boundary surface.

Consider the case $\nabla\Psi$ is pointing from the magnetic axis to the boundary flux surface, i.e., Ψ is increasing from the magnetic axis to the boundary magnetic surface. Since $\mathbf{B}_p = \nabla\Psi\times\nabla\phi$, the case corresponds to that B_p is count clockwise when the observer looks along the direction of $\nabla\phi$.

Using the coordinates transformation, equation (127) can be further written

$$\Psi = \frac{\mu_0 I}{4\pi a^2}\overline{R}[(R-\overline{R})^2+Z^2]. \tag{136}$$

Then the gradiant of Ψ is written

$$\nabla\Psi = \frac{\mu_0 I}{4\pi a^2}\overline{R}[2(R-\overline{R})\hat{\mathbf{R}}+2Z\hat{\mathbf{Z}}] \tag{137}$$

and the poloidal magnetic field is written

$$\begin{aligned}
\mathbf{B}_p &= \nabla\Psi\times\nabla\phi \\
&= \frac{\mu_0 I}{4\pi a^2}\overline{R}[2(R-\overline{R})\hat{\mathbf{R}}+2Z\hat{\mathbf{Z}}]\times\frac{1}{R}\hat{\boldsymbol{\phi}} \\
&= \frac{\mu_0 I}{4\pi a^2}\overline{R}\frac{1}{R}[2(R-\overline{R})\hat{\mathbf{Z}}-2Z\hat{\mathbf{R}}] \\
&= \frac{\mu_0 I}{4\pi a^2}\overline{R}\frac{2r}{R}[\cos\theta\hat{\mathbf{Z}}-\sin\theta\hat{\mathbf{R}}] \\
&= \frac{\mu_0 I}{4\pi a^2}\overline{R}\frac{2r}{R}\hat{\boldsymbol{\theta}}, \\
&= \frac{\mu_0 I}{4\pi a^2}\frac{2r}{1+\frac{r}{\overline{R}}\cos\theta}\hat{\boldsymbol{\theta}}.
\end{aligned} \tag{138}$$

where $\hat{\boldsymbol{\theta}}$ is the unit vector along the direction of increassing θ (count-clockwise when looking along $\nabla\phi$).

5 Equations of guiding-center motion—outdated, will be deleted

YJ's remark: This section is outdated because I have found a more accurate form of the equations of the guiding center motion, as given in Sec. 1. Besides to be more accurate, the new form is compact and suitable for numerical implemention

The equations for the guiding center motion are given by (refer to my note "collisionless_drift_kinetic_equation.tm")

$$\dot{\mathbf{X}} = v_\parallel\mathbf{b}+\frac{1}{\Omega}\mathbf{b}\times\left(\frac{\mu}{m}\nabla B+v_\parallel^2\boldsymbol{\kappa}\right), \tag{139}$$

and

$$\dot{v_\parallel} = -\frac{\mu}{m}\mathbf{b}\cdot\nabla B + v_\parallel \boldsymbol{\kappa}\cdot\dot{\mathbf{X}}, \tag{140}$$

where $\mu \equiv m v_\perp^2/(2B)$, $\mathbf{b} = \mathbf{B}/B$. The term $v_\parallel \boldsymbol{\kappa}\cdot\dot{\mathbf{X}}$ in Eq. (140) can be further simplified by using Eq. (139), which gives

$$\dot{v_\parallel} = -\frac{\mu}{m}\mathbf{b}\cdot\nabla B + \frac{v_\parallel \mu}{m\Omega}\boldsymbol{\kappa}\cdot\mathbf{b}\times\nabla B \tag{141}$$

where use has been made of that the curvature $\boldsymbol{\kappa}$ is perpendicular to $\mathbf{b}$.

[Benchmark: In GTC simulation (refer to H. Zhang's paper[6]), the time derivative of $v_\parallel$ is given by

$$\dot{v}_\parallel = -\frac{\mathbf{B} + B v_\parallel/\Omega_\alpha \nabla\times\mathbf{b}}{mB}\cdot\mu\nabla B \tag{142}$$

$$\Longrightarrow \dot{v}_\parallel = -\frac{\mu}{m}\mathbf{b}\cdot\nabla B - \frac{v_\parallel\mu}{m\Omega}\nabla\times\mathbf{b}\cdot\nabla B, \tag{143}$$

Next, I prove Eq. (141) is equivalent to Eq. (143). Using $\boldsymbol{\kappa} \equiv \mathbf{b}\cdot\nabla\mathbf{b} = -\mathbf{b}\times\nabla\times\mathbf{b}$, the second term on the right-hand side of Eq. (141) is written as

$$\begin{aligned}
\frac{v_\parallel\mu}{m\Omega}\boldsymbol{\kappa}\cdot\mathbf{b}\times\nabla B &= -\frac{v_\parallel\mu}{m\Omega}(\mathbf{b}\times\nabla\times\mathbf{b})\cdot(\mathbf{b}\times\nabla B) \\
&= -\frac{v_\parallel\mu}{m\Omega}\nabla\times\mathbf{b}\cdot\nabla B + \frac{v_\parallel\mu}{m\Omega}(\mathbf{b}\cdot\nabla B)(\nabla\times\mathbf{b}\cdot\mathbf{b}) \\
&\approx -\frac{v_\parallel\mu}{m\Omega}\nabla\times\mathbf{b}\cdot\nabla B + 0,
\end{aligned} \tag{144}$$

where in obtaining the last equality, use has been made of that $\nabla\times\mathbf{b}\cdot\mathbf{b}\approx 0$ (note that this is correct to the order considered here, I will discuss this later). Using Eq. (144) in Eq. (141) yields

$$\dot{v_\parallel} = -\frac{\mu}{m}\mathbf{b}\cdot\nabla B - \frac{v_\parallel\mu}{m\Omega}\nabla\times\mathbf{b}\cdot\nabla B, \tag{145}$$

which is identical with Eq. (143).]

5.1 Equations of guiding center motion in cylindrical coordinates-old, will be deleted

In the cylindrical coordinates (R, ϕ, Z), the location vector is written as

$$\mathbf{X} = R\hat{\mathbf{e}}_R + Z\hat{\mathbf{e}}_Z. \tag{146}$$

Using this, we obtain

$$\Rightarrow\dot{\mathbf{X}} = \dot{R}\hat{\mathbf{e}}_R + R\dot{\phi}\hat{\mathbf{e}}_\phi + \dot{Z}\hat{\mathbf{e}}_Z \tag{147}$$

Substituting this into the equation of motion gives

$$\dot{R}\hat{\mathbf{e}}_R + R\dot{\phi}\hat{\mathbf{e}}_\phi + \dot{Z}\hat{\mathbf{e}}_Z = v_\parallel\mathbf{b} + \frac{1}{\Omega}\mathbf{b}\times\Big(\frac{\mu}{m}\nabla B + v_\parallel^2\boldsymbol{\kappa}\Big). \tag{148}$$

The $\hat{\mathbf{e}}_R$ component of the above equation is written as

$$\dot{R} = v_\parallel b_R + \hat{\mathbf{e}}_R\cdot\frac{1}{\Omega}\mathbf{b}\times\Big(\frac{\mu}{m}\nabla B + v_\parallel^2\boldsymbol{\kappa}\Big). \tag{149}$$

Using

$$\begin{aligned}
\hat{\mathbf{e}}_R\cdot\frac{1}{\Omega}\mathbf{b}\times\frac{\mu}{m}\nabla B &= \frac{\mu}{m\Omega}\hat{\mathbf{e}}_R\cdot\mathbf{b}\times\nabla B \\
&= \frac{\mu}{m\Omega}\hat{\mathbf{e}}_R\cdot(b_R\hat{\mathbf{e}}_R + b_Z\hat{\mathbf{e}}_Z + b_\phi\hat{\mathbf{e}}_\phi)\times\left(\frac{\partial B}{\partial R}\hat{e}_R + \frac{\partial B}{\partial Z}\hat{e}_Z\right) \\
&= \frac{\mu}{m\Omega}b_\phi\frac{\partial B}{\partial Z}
\end{aligned} \tag{150}$$

and

$$\begin{aligned}
\hat{\mathbf{e}}_R\cdot\frac{1}{\Omega}\mathbf{b}\times v_\parallel^2\boldsymbol{\kappa} &= \frac{v_\parallel^2}{\Omega}\hat{\mathbf{e}}_R\cdot(\mathbf{b}\times\boldsymbol{\kappa}) \\
&= \frac{v_\parallel^2}{\Omega}\hat{\mathbf{e}}_R\cdot(b_R\hat{\mathbf{e}}_R + b_Z\hat{\mathbf{e}}_Z + b_\phi\hat{\mathbf{e}}_\phi)\times(\kappa_R\hat{e}_R + \kappa_Z\hat{e}_Z + \kappa_\phi\hat{e}_\phi) \\
&= \frac{v_\parallel^2}{\Omega}(-b_Z\kappa_\phi + b_\phi\kappa_Z),
\end{aligned} \tag{151}$$

Eq. (149) is written as

$$\dot{R} = v_\parallel b_R + \frac{\mu}{m\Omega}b_\phi\frac{\partial B}{\partial Z} + \frac{v_\parallel^2}{\Omega}(-b_Z\kappa_\phi + b_\phi\kappa_Z). \tag{152}$$

Equation (152) is used in my numerical code. The $\hat{\mathbf{e}}_Z$ component of Eq. (148) is written as

$$\dot{Z} = v_\parallel b_Z + \hat{\mathbf{e}}_Z\cdot\frac{1}{\Omega}\mathbf{b}\times\Big(\frac{\mu}{m}\nabla B + v_\parallel^2\boldsymbol{\kappa}\Big). \tag{153}$$

Using

$$\begin{aligned}\hat{\mathbf{e}}_Z\cdot\frac{1}{\Omega}\mathbf{b}\times\frac{\mu}{m}\nabla B &= \frac{\mu}{m\Omega}\hat{\mathbf{e}}_Z\cdot\mathbf{b}\times\nabla B\\ &= \frac{\mu}{m\Omega}\hat{\mathbf{e}}_Z\cdot(b_R\hat{\mathbf{e}}_R+b_Z\hat{\mathbf{e}}_Z+b_\phi\hat{\mathbf{e}}_\phi)\times\left(\frac{\partial B}{\partial R}\hat{e}_R+\frac{\partial B}{\partial Z}\hat{e}_Z\right)\\ &= -\frac{\mu}{m\Omega}b_\phi\frac{\partial B}{\partial R}\end{aligned}\tag{154}$$

and

$$\begin{aligned}\hat{\mathbf{e}}_Z\cdot\frac{1}{\Omega}\mathbf{b}\times v_\parallel^2\boldsymbol{\kappa} &= \frac{v_\parallel^2}{\Omega}\hat{\mathbf{e}}_Z\cdot\mathbf{b}\times\boldsymbol{\kappa}\\ &= \frac{v_\parallel^2}{\Omega}\hat{\mathbf{e}}_Z\cdot(b_R\hat{\mathbf{e}}_R+b_Z\hat{\mathbf{e}}_Z+b_\phi\hat{\mathbf{e}}_\phi)\times(\kappa_R\hat{e}_R+\kappa_Z\hat{e}_Z+\kappa_\phi\hat{e}_\phi)\\ &= \frac{v_\parallel^2}{\Omega}(b_R\kappa_\phi-b_\phi\kappa_R),\end{aligned}\tag{155}$$

Eq. (153) is written as

$$\dot{Z}=v_\parallel b_Z-\frac{\mu}{m\Omega}b_\phi\frac{\partial B}{\partial R}+\frac{v_\parallel^2}{\Omega}(b_R\kappa_\phi-b_\phi\kappa_R).\tag{156}$$

Equation (156) is used in my numerical code.

Next we consider the equation for the time evolution of $v_\parallel$, Eq. (141), i.e.,

$$\dot{v_\parallel}=-\frac{\mu}{m}\mathbf{b}\cdot\nabla B+\frac{v_\parallel\mu}{m\Omega}\boldsymbol{\kappa}\cdot\mathbf{b}\times\nabla B.\tag{157}$$

The first term of on the right-hand side of Eq. (157) can be written as

$$\begin{aligned}-\frac{\mu}{m}\mathbf{b}\cdot\nabla B &= -\frac{\mu}{m}(b_R\hat{e}_R+b_Z\hat{e}_Z+b_\phi\hat{e}_\phi)\cdot\left(\frac{\partial B}{\partial R}\hat{e}_R+\frac{\partial B}{\partial Z}\hat{e}_Z\right)\\ &= -\frac{\mu}{m}\left(b_R\frac{\partial B}{\partial R}+b_Z\frac{\partial B}{\partial Z}\right).\end{aligned}\tag{158}$$

The second term on the right-hand side of Eq. (157) can be written as

$$\begin{aligned}\boldsymbol{\kappa}\cdot[\mathbf{b}\times\nabla B] &= (\kappa_R\hat{e}_R+\kappa_Z\hat{e}_Z+\kappa_\phi\hat{e}_\phi)\cdot\left[(b_R\hat{e}_R+b_Z\hat{e}_Z+b_\phi\hat{e}_\phi)\times\left(\frac{\partial B}{\partial R}\hat{e}_R+\frac{\partial B}{\partial Z}\hat{e}_Z\right)\right]\\ &= (\kappa_R\hat{e}_R+\kappa_Z\hat{e}_Z+\kappa_\phi\hat{e}_\phi)\cdot\left[-b_R\frac{\partial B}{\partial Z}\hat{e}_\phi+b_Z\frac{\partial B}{\partial R}\hat{e}_\phi-b_\phi\frac{\partial B}{\partial R}\hat{e}_Z+b_\phi\frac{\partial B}{\partial Z}\hat{e}_R\right]\\ &= \kappa_R b_\phi\frac{\partial B}{\partial Z}-\kappa_Z b_\phi\frac{\partial B}{\partial R}+\kappa_\phi\left(b_Z\frac{\partial B}{\partial R}-b_R\frac{\partial B}{\partial Z}\right).\end{aligned}\tag{159}$$

Using these results, Eq. (157) is written as

$$\dot{v_\parallel}=-\frac{\mu}{m}\left(b_R\frac{\partial B}{\partial R}+b_Z\frac{\partial B}{\partial Z}\right)+\frac{\mu v_\parallel}{m\Omega}\left[\kappa_R b_\phi\frac{\partial B}{\partial Z}-\kappa_Z b_\phi\frac{\partial B}{\partial R}+\kappa_\phi\left(b_Z\frac{\partial B}{\partial R}-b_R\frac{\partial B}{\partial Z}\right)\right].\tag{160}$$

Equation (160) is used in my numerical code.

Next consider the $\hat{\mathbf{e}}_\phi$ component of Eq. (148), which is written as

$$R\dot{\phi}=v_\parallel b_\phi+\frac{1}{\Omega}\hat{\mathbf{e}}_\phi\cdot\left[\mathbf{b}\times\left(\frac{\mu}{m}\nabla B+v_\parallel^2\boldsymbol{\kappa}\right)\right].\tag{161}$$

Using

$$\begin{aligned}\frac{1}{\Omega}\hat{\mathbf{e}}_\phi\cdot\left(\mathbf{b}\times\frac{\mu}{m}\nabla B\right) &= \frac{\mu}{\Omega m}\hat{\mathbf{e}}_\phi\cdot(\mathbf{b}\times\nabla B)\\ &= \frac{\mu}{\Omega m}\hat{\mathbf{e}}_\phi\cdot\left[(b_R\hat{\mathbf{e}}_R+b_Z\hat{\mathbf{e}}_Z)\times\left(\frac{\partial B}{\partial R}\hat{e}_R+\frac{\partial B}{\partial Z}\hat{e}_Z\right)\right]\\ &= \frac{\mu}{\Omega m}\left(-b_R\frac{\partial B}{\partial Z}+b_Z\frac{\partial B}{\partial R}\right),\end{aligned}\tag{162}$$

and

$$\begin{aligned}\frac{v_\parallel^2}{\Omega}\hat{\mathbf{e}}_\phi\cdot\mathbf{b}\times\boldsymbol{\kappa} &= \frac{v_\parallel^2}{\Omega}\hat{\mathbf{e}}_\phi\cdot\left(b_R\hat{\mathbf{e}}_R+b_Z\hat{\mathbf{b}}_Z\right)\times\left(\kappa_R\hat{\mathbf{e}}_R+\kappa_Z\hat{\mathbf{b}}_Z\right)\\ &= \frac{v_\parallel^2}{\Omega}(-b_R\kappa_Z+b_Z\kappa_R),\end{aligned}\tag{163}$$

Eq. (161) is written as

$$R\dot{\phi}=v_\parallel b_\phi+\frac{\mu}{\Omega m}\left(-b_R\frac{\partial B}{\partial Z}+b_Z\frac{\partial B}{\partial R}\right)+\frac{v_\parallel^2}{\Omega}(-b_R\kappa_Z+b_Z\kappa_R).\tag{164}$$

Equation (164) (in normalized form) is used in my numerical code.

Bibliography

[1] Y. Todo. Properties of energetic-particle continuum modes destabilized by energetic ions with beam-like velocity distributions. *Phys. Plasmas (1994-present)*, 13(8):–, 2006.

[2] John Wesson. *Tokamaks*. Oxford University Press, 2004.

[3] Z. Lin, W. M. Tang, and W. W. Lee. Gyrokinetic particle simulation of neoclassical transport. *Physics of Plasmas*, 2(8):2975, 1995.

[4] Allen H. Boozer. Physics of magnetically confined plasmas. *Rev. Mod. Phys.*, 76:1071–1141, Jan 2005.

[5] Shaojie Wang. Finite bootstrap current density and finite neoclassical reduction of electrical conductivity at the magnetic axis of a tokamak. *Phys. Fluids*, 5(9):3319–3324, 1998.

[6] H. S. Zhang, Z. Lin, I. Holod, X. Wang, Y. Xiao, and W. L. Zhang. Gyrokinetic particle simulation of beta-induced alfvén eigenmode. *Phys. Plasmas*, 17(11):112505, 2010.